Hole dynamics in doped cuprates: High-T_c superconductivity originated from antiferromagnetic exchange as a direct attractive interaction

F. Onufrieva, S. Petit, and Y. Sidis
Laboratoire Leon Brillouin, CE-Saclay 91191, Gif-sur-Yvette, France
(Received 30 January 1996; revised manuscript received 26 June 1996)

A strong-coupling-limit theory of hole dynamics in copper oxide superconductors is developed. The theory is based on the t-t'-J model and the diagrammatic technique for projection operators. For the normal state two different phases at finite temperature are found. For the first (which is realized at low doping), a Fermi surface (FS) is formed by doped holes only and so has a volume proportional to δ, while d electrons are responsible for a localized magnetism. For the second (which is realized at intermediate doping), the d electrons become a part of the FS the volume of which is proportional to $1+\delta$, while the system loses the magnetic moments associated with d electrons. A transition between the two phases is of first order and the FS changes abruptly from a small to a large one. The phase with the small FS is unstable when lowering the temperature in as much as a spin susceptibility diverges at $\mathbf{k}=\mathbf{Q}_{\mathrm{AF}}$. Therefore, at low temperature within the doping range corresponding to this phase, a long-range antiferromagnetic (AF) ground state or quantum-disordered ground state is realized depending on doping. Most attention in the paper is paid to the second state characterized by a saddle-point (SP) singularity and a large Fermi surface. Self-consistent calculations for the chemical potential show that at some critical doping which depends on the ratio of hopping parameters t'/t, the Fermi level crosses the SP. For this phase, a short-distance superconducting (SC) pairing of d-wave symmetry with a large amplitude of the SC gap is found at low temperature. The critical temperature is very high. The superconducting pairing has a magnetic origin but the mechanism is different from an exchange by spin waves. The mechanism is related to the AF exchange between localized spins, turning out to be a direct attractive interaction between carriers. The latter point is a consequence of the specific nature of carriers appearing as a result of strong on-site Coulomb repulsion. On the other hand, the specific kinematic properties of the carriers create a strong constraint on symmetry of the superconducting order parameter which eliminates all symmetries without nodes and favors strongly d-wave symmetry. In such a situation the existence of a saddle point close to the Fermi level is a factor providing a maximum value of the effective interaction. An interrelation between an extension of the SP singularity and a value of the amplitude of the SC gap is analyzed; a saturation effect is found. [S0163-1829(96)05238-1]

I. INTRODUCTION

Since the discovery of high-T_c superconductivity, different scenarios have been proposed to explain this phenomenon. Recently the discussion has been concentrated on two points: first, on the importance of a saddle point or an extended saddle-point singularity in the electronic spectrum in the normal state irrespective of the nature of the superconducting (SC) pairing and, second, on the potentially important role of magnetic degrees of freedom in the pairing mechanism.

Apart from phenomenological studies (see, for example, Refs. 1–5), a microscopic mechanism of magnetic origin usually considered is a virtual exchange by spin waves which leads to an attractive interaction between carriers.[6–8] In these theoretical descriptions, both spin and hole degrees of freedom are considered on the basis of an antiferromagnetic (AF) state that implies long-range (LR) ordering for the localized-spin degrees of freedom and the Fermi surface (FS) forming small hole pockets around $(\pm\pi/2,\pm\pi/2)$ for the charge degrees of freedom. Although superconductivity and antiferromagnetism do not coexist in the high-T_c superconductors, such an approach could be considered as qualitatively relevant if (i) the paramagnetic metallic state above T_c were characterized by a short-range (SR) AF ordering with a quite large magnetic correlation length ξ_{AF}, (ii) the intensity of the dynamic spin susceptibility in this state were considerable and its variation with doping would correlate somehow with the doping dependence of T_c, and (iii) the dispersion law of carriers and their Fermi surface (FS) in the metallic state of interest (i.e., for the hole concentration corresponding to the existence of superconductivity) were qualitatively close to the dispersion law and FS of one hole on the AF background.

However, different experiments performed on the hole-doped cuprates appear to prove the opposite. Angle-resolved photoemission electron spectroscopy (ARPES) experiments which probe a hole dynamics show that the spectrum of a photohole on the antiferromagnetic background observed in insulating $Sr_2CuO_2Cl_2$ (Ref. 9) indeed corresponds to the FS with the small hole pockets centered at $(\pm\pi/2,\pm\pi/2)$. Meanwhile, for the doping corresponding to the superconductivity, the picture is quite different; the large hole pockets centered at $(\pm\pi,\pm\pi)$ are observed in the metallic state above T_c.[10–18] The difference between the hole dynamics in the paramagnetic state above T_N and above T_c is especially impressive in the experiments performed on the same crystal in continuously changing doping,[11] namely, in

$YBa_2Cu_3O_{6+x}$ (YBCO) with $x=0.35$ corresponding to the insulating AF state and with $x=0.4,0.5,0.7,0.9$ corresponding to the metallic state. (In this series of experiments the data for insulating, but not carrier-free, $YBa_2Cu_3O_{6.35}$ are consistent with the results in $Sr_2CuO_2Cl_2$, and the data for the metallic $YBa_2Cu_3O_{6+x}$ with $x=0.4,0.5,0.7,0.9$ are consistent with data for the other hole-doped cuprates in the metallic state.) Thus, the ARPES data seem to indicate that condition (iii) is not satisfied. Nevertheless, the situation from ARPES is not absolutely clear due to the effect of shadow bands observed in $Bi_2Sr_2CaCu_2O_{8+x}$ (Bi2212).[19,20] Being interpreted as a signature of SR AF ordering (and being assumed that this ordering is close to the LR AF ordering in the insulating state) this discovery just motivated Refs. 6–8. (It should be noticed, however, that the interpretation of the shadow-band effect is controversial; it can be merely explained as having a structural origin,[21] as has been noted in Refs. 19 and 20. On the other hand, even if it were confirmed that the effect is a consequence of SR AF correlations, there is no reason to identify the latter with spin waves in the LR AF insulating state. It is more natural to think about specific fluctuations of the quantum-spin-liquid type.)

There is, however, another type of experiment which clarifies the situation. This is a neutron scattering experiment which probes directly the magnetic ordering and spin dynamics. The results of such experiments indicate clearly that conditions (i) and (ii) are not satisfied. Firstly, as has been discovered, the magnetic correlation length ξ_{AF} in the normal state above T_c is extremely small.[22–25] For example, in the case of YBCO, $\xi_{AF}\approx 4$ Å (which is of the order of *one unit cell*) for the doping $x=0.92$ just corresponding to the maximum T_c (= 92 K).[23] Second, the intensity of the observed inelastic neutron scattering (INS) signal, which is proportional to the imaginary part of the dynamic spin susceptibility, $\mathrm{Im}\chi(Q_{AF},\omega)$, decreases with doping within the metallic state[24] (while T_c increases) and drops almost to zero for the doping $x=1$,[26–28] while the value of T_c is almost maximum, $T_c=90$ K. Third, there is clear evidence for a strong qualitative change of the spin dynamics between the LR AF state and the metallic state above T_c (see, for example, the experiments of the group of J. Rossat-Mignod which have been progressively performed on the same crystal $YBa_2Cu_3O_{6+x}$ in continuously changing doping from the insulating to the superconducting state (for the insulating state see Refs. 29–31, for the weakly doped metallic state see Refs. 32–34 and for the heavily doped state see Refs. 32 and 35–37). As was emphasized in the review paper in Ref. 38, inelastic neutron scattering clearly indicates that the propagative spin-wave excitations disappear when one passes from the LR AF state to the metallic state but instead a broad in energy and weakly temperature-dependent spectrum is observed.

All these features make doubtful, first, the use of the basis corresponding to the LR AF state for a microscopical explanation of high-T_c superconductivity phenomena and, second, more generally, the scenario of the exchange by spin waves itself. On the other hand, a magnetic origin of superconducting pairing in high-T_c cuprates is believed to be more and more probable due to a mounting evidence for a d-wave symmetry of the superconducting order parameter.[39–43]

In the present paper we show that a natural mechanism for superconducting pairing of magnetic origin exists, different from exchange by spin waves, but still related to the existence of localized spins with a strong AF interaction in the CuO_2 plane. Moreover, this mechanism leads to a high value of the amplitude of the SC gap, and so of T_c, and to the $d_{x^2-y^2}$ symmetry of the superconducting order parameter (SC OP). This mechanism can be qualitatively explained as follows. The first important point is the specific nature of the propagating charged quasiparticles in the CuO_2 plane. As was first shown by Zhang and Rice[44] and then by other authors,[45,46] it is energetically favorable for a doped hole on oxygen to create a singlet bound state with a hole on Cu within the square plaquette. The motion of the extra hole through the lattice occurs as follows: The extra hole creates a singlet on site i, and when the carrier hops on another site j, a free Cu spin is restored on site i.[47] This way, the itinerant charged quasiparticles are in a strong connection with the localized-spin subsystem. As we show later on, this peculiarity of the carriers, arising from the effect of strong electron correlations, yields the second important point: *The AF exchange between the localized spins turns out to be a direct attractive interaction between these quasiparticles.* The next point is the shape and the volume of the FS of the considered quasiparticles: Above some critical doping the FS is large, contrary to the above-mentioned microscopical theories,[6–8] and the spectrum is characterized by a saddle point (SP) or an extended SP (depending on the values of hopping parameters) whose energy for the doping range $\delta=0.1-0.3$ turns out to be close to the Fermi level (δ is the concentration of doped holes per Cu within the CuO_2 plane). Then, the anisotropy of the attractive interaction, on the one hand, together with the large FS and the existence of the SP singularity close to Fermi level, on the other hand, lead to the $d_{x^2-y^2}$ symmetry of the superconducting order parameter and, moreover, to high values of the amplitude of the SC gap.[49] The last important point is the evolution of this picture with doping. The doping dependence of the chemical potential occurs in such a way that it crosses the saddle point at some doping δ_c whose value depends on the ratio t'/t where t is a nearest-neighbor hopping term and t' is a next-nearest-neighbor hopping term. The maximum of T_c is reached around $\delta=\delta_c$ and T_c decreases at higher or lower doping. The explicit doping dependences of T_c turn out to be close to those observed experimentally for monolayer and bilayer cuprates, as well as the values of the maximum amplitude of the SC gap and the values of the maximum of T_c. It is worth noting, in addition, that the evolution of the FS with doping in the normal state, namely, its abrupt change from a small FS with the volume proportional to δ to a large FS with the volume proportional to $1+\delta$ obtained within the theory, is also close to that observed experimentally. It allows us, as we hope, to shed light on the striking change of the shape and volume of the FS between the insulating and metallic states observed by ARPES.

The paper is organized as follows. In Sec. II, we describe the model, namely, the t-t'-J model which is the simplest relevant model for the CuO_2 plane. We treat this model within the diagrammatic technique (DT) for Hubbard operators.[54–56] (So far as the present work is a continuation of Ref. 57, details about the formalism can be found therein.) The hole and spin dynamics in the normal state are analyzed

in Sec. III. In Sec. IV we present the equation for the SC gap and its solutions for the cases of different FS's. We analyze the symmetry of the SC OP and the amplitude of the SC gap as a function of doping. Section V contains our conclusions. Some mathematical details which are necessary to understand our results are presented in the Appendix.

II. MODEL: LIE-HUBBARD OPERATORS

We use the same model as in Refs. 6–8, the t-t'-J model which is the simplest model incorporating the issue of strong electron correlations within the CuO_2 plane. It was derived from the realistic three-band Hubbard model for the CuO_2 plane with the idea of the local singlet and of the Wannier representation for O states.[44–48] Within this model, the CuO_2 plane is treated as a lattice of square plaquettes centered on Cu sites with four surrounding oxygens, and only three low-energy states are taken into account. Those are the two states corresponding to a single hole with spin up and down, $|1\rangle$ and $|-1\rangle$, and the one state corresponding to the singlet state of two holes, $|0\rangle$.[58] Being the simplest one in the family of strong-coupling-limit models, this model is quite good for describing low-energy excitations in the CuO_2 plane; the energy distances to other levels of the plaquette are very large. For example, the distance between the singlet and triplet two-hole states is approximately 3.6–3.7 eV; see the most recent and accurate calculations in Ref. 48.

Like all other strong-coupling-limit models, the t-J model is formulated in terms of projection operators (or X operators, or Hubbard operators) defined as describing transitions between different states of the plaquette,

$$X_i^{\lambda\mu}=|\lambda\rangle\langle\mu|. \tag{1}$$

The Hamiltonian is written as

$$H=H_0+H_t+H_J, \tag{2}$$

$$H_t=\sum_{ij}\ t_{ij}\{X_i^{01}X_j^{10}+X_i^{0-1}X_j^{-10}\}, \tag{3}$$

$$H_J=\sum_{ij}\ J_{ij}\{X_i^{1-1}X_j^{-11}-X_i^{11}X_j^{-1-1}\}, \tag{4}$$

$$H_0=\sum_i\ E_0X_i^{00}+E_\sigma(X_i^{-1-1}+X_i^{11})-\frac{h}{2}(X_i^{11}-X_i^{-1-1}). \tag{5}$$

Keeping in mind the definition (1) of X operators, one can see that the Hamiltonian H_t describes the motion of the doped hole which creates a singlet state on one site and restores a free spin of the localized hole on another. The Hamiltonian H_J describes the exchange interaction between localized spins. The on-site Hamiltonian H_0 describes the energies of the different states of the plaquette; it includes as well an external magnetic field term. In the paper we will consider the model with the hopping between nearest (t), next-nearest (t'), and third neighbors (t'').

The point that the model is formulated in terms of the projection operators (1) is very important. These operators are neither Fermi nor Bose operators; they form a complete algebra with specific multiplication rules

$$X_i^{\lambda\mu}X_i^{\nu\rho}=\delta_{\mu\nu}X_i^{\lambda\rho}, \tag{6}$$

commutation relations[59]

$$[X_i^{\lambda\mu},X_j^{\nu\rho}]_\pm=\delta_{ij}(X_i^{\lambda\rho}\delta_{\mu\nu}\pm X_i^{\nu\mu}\delta_{\rho\lambda}), \tag{7}$$

and a conservation rule

$$\sum_\lambda\ X_i^{\lambda\lambda}=1. \tag{8}$$

[The conjugated operators are related as follows: $(X_i^{\lambda\mu})^+=X_i^{\mu\lambda}$.] For the same-site operators this algebra is a Lie algebra SU(3); different-site X operators are Bose-like or Fermi-like depending on the sign in Eq. (7).[59]

The properties of X operators reflect the interrelation between different degrees of freedom, in our case between the localized spins and the itinerant holes. Indeed, the localized-spin operator $S_j^-\equiv X_j^{-11}$ can be represented as a product of two-hole operators, $X_j^{-11}=X_j^{-10}X_j^{01}$, and the hole operator X_j^{01} as a product of the spin operator and the hole operator with another spin, $X_j^{10}=X_j^{1-1}X_j^{-10}$ etc. The interrelation between different degrees of freedom is, however, lost when the exact algebra (6)–(8) is reduced to the algebra of Bose-Fermi operators by using any auxiliary representation for X operators, the slave boson, the slave fermion, and others.[60] Depending on the type of auxiliary representation, the t-J model turns out to be reduced to different models corresponding to different limiting cases, for example, to the normal-metal limit, to the spin-charge-separation limit, to the limit of long-range-ordered magnetic states, etc. This point has been analyzed in Ref. 57; see Appendix A therein.

In fact, the problem is much more general. All models in different branches of physics which start with states of one cluster (or one atom, one molecule, one spin) are formulated in terms of projection operators. Those are, for example, the models describing excitons in molecular crystals,[61] the models describing the propagating intramolecular excitations in quantum molecular crystals, vibrons, and librons,[62] the models describing spin fluctuations in localized-spin systems,[63] the Heisenberg, the X-Y, the Ising models, etc. The peculiarity of the algebra of X operators is intrinsic; it results in intrinsic differences between quasiparticles associated with Fermi-Bose operators and quasiparticles associated with X operators.[64] In the following we will call these operators Lie-Hubbard (LH) operators for the following reasons. On the one hand, their peculiarities and the peculiarities of quasiparticles associated with them for arbitrary models are completely determined by the properties of the Lie algebra. On the other hand, in physics they are more known as Hubbard operators after their introduction by Hubbard in his four-state particular model. We will also call the quasiparticles associated with LH operators lieons to emphasize their profound difference from fermions and bosons. Depending on commutation relations for different-site operators, there are Bose-like and Fermi-like LH operators. Spin operators are another case of Bose-like LH operators and spin waves are particular case of lieons.

In order to fully comprehend the specificity of kinematic properties of quasiparticles associated with LH operators, lieons, it is very important to work accurately with the models formulated in terms of these operators, namely, to use a formalism which does not destroy their algebra.[65] One of such formalism is the diagrammatic technique (DT) for Hubbard operators[54–56] which we will use in the present paper. We will analyze simultaneously the hole and spin dynamics which are associated with Matsubara's hole and spin Green functions determined as follows:

$$G^{s}(\mathbf{k},i\omega_n)=\langle\langle X_{\mathbf{k}}^{\sigma\overline{\sigma}}|X_{-\mathbf{k}}^{\overline{\sigma}\sigma}\rangle\rangle_{i\omega_n}=\int_{-\beta}^{\beta}d\tau\,\exp(-i\omega_n\tau)\langle T_\tau X_{\mathbf{k}}^{\sigma\overline{\sigma}}(\tau)X_{-\mathbf{k}}^{\overline{\sigma}\sigma}(0)\rangle, \tag{9}$$

$$G_{\sigma\sigma}^{h}(\mathbf{k},i\omega_n)=\langle\langle X_{\mathbf{k}}^{\sigma 0}|X_{-\mathbf{k}}^{0\sigma}\rangle\rangle_{i\omega_n}=\int_{-\beta}^{\beta}d\tau\,\exp(-i\omega_n\tau)\langle T_\tau X_{\mathbf{k}}^{\sigma 0}(\tau)X_{-\mathbf{k}}^{0\sigma}(0)\rangle. \tag{10}$$

In Eqs. (9) and (10), ω_n are Matsubara frequencies, T_τ is the chronological operator, τ is the imaginary time, $X^{pq}(\tau)$ are X operators in the interaction representation, and $\sigma,\overline{\sigma}=1,-1$. The spin Green function describes the localized spins whereas the hole Green function describes itinerant quasiparticles which correspond to the motion of the doped holes creating the singlet state on one site and restoring a free spin of the localized hole on another site. We will use the analytical expressions for the spin Green function and the normal-state hole Green function obtained in Refs. 69 and 57 for the doped antiferromagnetic state in CuO_2 plane and the paramagnetic metallic state with short-range AF correlations, respectively. Since the corresponding expressions for the case of the doped AF state have been obtained in Ref. 69 by using the auxiliary representation corresponding to LR AF ordering, we show in the Appendix how these expressions appear within the DT for LH operators.

III. HOLE DYNAMICS IN THE NORMAL STATE

As was discussed in Ref. 57, the exact structure of both spin and hole Green functions in the DT for X operators is given by the Larkin equation

$$G(\mathbf{k},i\omega_n)=\frac{\Sigma(\mathbf{k},i\omega_n)}{1-V_{\mathbf{k}}\Sigma(\mathbf{k},i\omega_n)}, \tag{11}$$

which is an analog of the Dyson equation in the diagrammatic technique for Bose or Fermi operators. In Eq. (11), $\Sigma(\mathbf{k},i\omega_n)$ is an irreducible part of diagram which cannot be cut along an interaction line (in the contrast to the Dyson equation where the self-energy is an irreducible part which cannot be cut along a Green-function line). $V_{\mathbf{k}}$ is an interaction potential which is equal to

$$V_{\mathbf{k}}^{s}=-J_{\mathbf{k}}=-4J\gamma_{\mathbf{k}} \tag{12}$$

for the case of the spin Green function and to

$$V_{\mathbf{k}}^{h}=-t_{\mathbf{k}}=-4t\gamma_{\mathbf{k}}-4t'\eta_{\mathbf{k}} \tag{13}$$

for the case of the hole Green function, where

$$\gamma_{\mathbf{k}}=\tfrac{1}{2}(\cos k_x+\cos k_y),\quad \eta_{\mathbf{k}}=\cos k_x\cos k_y. \tag{14}$$

The irreducible part should be calculated in some order of the perturbation theory with respect to $H_{\rm int}=H-H_0$, where H_0 includes on-site terms and $H_{\rm int}$ includes intersite terms. The perturbation theory with respect to $H_{\rm int}$ means in the considered case the perturbation theory with respect to small parameters $1/z$, where z is the number of nearest neighbors.

A. Hole and spin Green functions in the case of the paramagnetic state

For the normal state without LR magnetic ordering (paramagnetic state), the hole irreducible part $\Sigma_{\sigma\sigma}^{h}(k,i\omega_n)$ in zero-order approximation is given by[57]

$$\Sigma_{\sigma\sigma}^{h(0)}(\mathbf{k},i\omega_n)=G_{\sigma\sigma}^{h(0)}(i\omega_n)=\frac{b^{\sigma 0}}{-\mu-i\omega_n^F}, \tag{15}$$

and, respectively, the hole Green function determined by Eqs. (11) and (13) is written as

$$G_{\sigma\sigma}^{h}(\mathbf{k},i\omega_n)=b^{\sigma 0}K_{\sigma\sigma}^{h}(\mathbf{k},i\omega_n),$$

$$K_{\sigma\sigma}^{h}(\mathbf{k},i\omega_n)=\frac{1}{\epsilon_{\mathbf{k}\sigma}-\mu-i\omega_n^F}, \tag{16}$$

$$\epsilon_{\mathbf{k}\sigma}=\frac{1+\delta}{2}\{(2t(\cos k_x+\cos k_y)+4t'\cos k_x\cos k_y\}. \tag{17}$$

In Eqs. (15)–(17), $G_{\sigma\sigma}^{h(0)}(i\omega_n)$ is a Green function corresponding to on-site Hamiltonian H_0 and $b^{\sigma 0}$ is a first-order cumulant determined as

$$b^{\sigma 0}=\langle[X_i^{\sigma 0},X_i^{0\sigma}]_+\rangle=\langle X_i^{00}+X_i^{\sigma\sigma}\rangle \tag{18}$$

and so given by

$$b^{\sigma 0}=\frac{1+\delta}{2}, \tag{19}$$

where δ is the number of doped holes per unit cell within CuO_2 plane ($\langle X^{00}\rangle=\delta$), μ is an effective chemical potential (which includes also on-site energies E_0 and E_σ), and $\omega_n^F=(2n+1)\pi T$ are Fermi-type Matsubara frequencies. The Green function $K_{\sigma\sigma}^{h}$ describes some effective fermions which have the same dispersion law as physical quasiparticles described by $G_{\sigma\sigma}^{h}$.[70] This dispersion law is given by Eq. (17); the factor $(1+\delta)/2$ related to the first-order cumulant $b^{\sigma 0}$ is important, for it leads to a narrowing of bandwidth and to its dependence on doping as we discuss later on.

The spin irreducible part $\Sigma^{s}(\mathbf{k},i\omega_n)$ in a zero-order approximation is written as[57]

$$\Sigma^{s(0)}(\mathbf{k},i\omega_n)=G^{s(0)}(i\omega_n)=\frac{b^{\sigma\overline{\sigma}}}{h-i\omega_n^B}, \tag{20}$$

where $G^{s(0)}(i\omega_n)$ is a spin Green function corresponding to a zeroth on-site Hamiltonian, the first-order cumulant $b^{\sigma\overline{\sigma}}$ is determined as

$$b^{\sigma\bar{\sigma}} = \langle [X_i^{\sigma\bar{\sigma}}, X_i^{\bar{\sigma}\sigma}]_- \rangle = \langle X_i^{\sigma\sigma} - X_i^{\bar{\sigma}\bar{\sigma}} \rangle, \quad (21)$$

and the Matsubara frequencies of Bose-type are given by $\omega_n^B = 2n\pi T$. Calculations in the limit of $h \to 0$ give us

$$\Sigma^{s(0)} = \delta_{\omega_n,0} \frac{C(T)}{T}, \quad C(T) = \frac{1}{2 + \exp(\mu/T)}. \quad (22)$$

Respectively, the spin Green function in this approximation is written as follows:

$$G^s(\mathbf{k}, i\omega_n) = \delta_{\omega_n,0} \frac{C(T)}{T + J_{\mathbf{k}} C(T)}. \quad (23)$$

Expressions (16) and (23) for the hole and spin Green functions correspond to a zero-order approximation for the hole and spin irreducible parts. This is the lowest approximation in the DT for Hubbard operators (HO's) in which quasiparticles described by Green functions become propagating. The first-order corrections to $\Sigma^h_{\sigma\sigma}(\mathbf{k}, i\omega_n)$ and $\Sigma^s(\mathbf{k}, i\omega_n)$ and the corresponding expressions for the hole and spin Green functions are given in Ref. 57. The important point for the present consideration is that the hole Green function is represented as a sum of coherent and incoherent parts:

$$G^h_{\sigma\sigma}(\mathbf{k}, i\omega_n) = G^{h(\mathrm{coh})}_{\sigma\sigma}(\mathbf{k}, i\omega_n) + G^{h,(\mathrm{inc})}_{\sigma\sigma}(\mathbf{k}, i\omega_n), \quad (24)$$

where $G^{h(\mathrm{coh})}_{\sigma\sigma}$ has a structure similar to Eq. (16) with a renormalized residue and dispersion law:

$$G^{h(\mathrm{coh})}_{\sigma\sigma}(\mathbf{k}, i\omega_n) = \frac{Z b^{\sigma 0}}{\tilde{\epsilon}_{\mathbf{k}\sigma} - \mu - i\omega_n^F}. \quad (25)$$

As to the spin Green function, there are also other contributions to the irreducible part Σ^s (we have analyzed the spin dynamics in detail in Ref. 57). However, the most important term for the present aim is just the simplest, static, contribution $\Sigma^{s(0)}$ given by Eqs. (20)–(22), since just this term behaves qualitatively differently for two kinds of normal-state hole dynamics as we shall see later on.

The equation for the chemical potential in the first-order approximation with respect to $1/z$ and in the limit of low temperature[71] has been obtained in Ref. 57. It is given by:[72]

$$\langle X^{00} \rangle = m + \frac{1}{N} \sum_{\mathbf{k},\sigma} \{ n^F(\epsilon_{\mathbf{k}\sigma} - \mu) - n^F(-\mu) \}, \quad (26)$$

$$m = \frac{1}{1 + 2\ \exp(-\mu/T)}, \quad (27)$$

where $n^F(x)$ is the Fermi function. The first term in Eq. (26) arises from the on-site terms of the Hamiltonian while the second one is related to the hole hopping.

B. Hole and spin Green functions in the case of the antiferromagnetic ground state

For the AF ground state, an additional contribution to the zero-order spin irreducible part Σ^s exists. It is related to the internal magnetic field corresponding to the AF ordering. In the case of two-sublattice AF ordering, $\Sigma^{s(0)}$ is a 2×2 matrix and the Larkin equation has a matrix form

$$\hat{G} = (\hat{I} - \hat{\Sigma}\hat{V})^{-1}\hat{\Sigma}. \quad (28)$$

The explicit expressions for $\hat{V}^s$ and $\hat{\Sigma}^{s(0)}$ are given in the Appendix; see Eqs. (A3) and (A2). When this contribution is dominant in comparison with other contributions to Σ^s (pure AF state in the undoped cuprates), the spin Green function acquires the usual spin-wave structure; see Eqs. (A4)–(A8) in the Appendix.

The hole Green function in the AF state is a 2×2 matrix as well. It is determined by the Larkin equation (28) with the interaction matrix given by Eq. (A14) and the irreducible part which in the zero-order approximation is given by Eq. (A17). Due to the fact that the first-order cumulant $b^{\sigma 0}$ is equal to unity for a lattice site belonging to one sublattice, but is vanishingly small for a site belonging to the other, the term in the denominator of the Larkin equation associated with the interaction potential is vanishingly small (see the Appendix). The hole Green function is written as

$$G^{h(0)}_{\sigma\sigma} \approx \Sigma^{h(0)}_{\sigma\sigma} \quad (29)$$

[where $\Sigma^{h(0)}_{\sigma\sigma}$ is determined by Eq. (A17)] and thus the holes are not propagating quasiparticles. The physical reason for this is that the existence of a rigid AF structure forbids a direct hopping of the doped hole to a nearest-neighbor site. This occurs when $t' = 0$. The propagation of the doped hole is, however, possible within the same sublattice, for in this case $b^{\sigma 0}$ is of the order of unity for all sites. Such a propagation occurs in the approximation considered when the hopping to the next nearest neighbors t' is not equal to zero [see Eqs. (A19) and (A20) and Refs. 69 and 73] and in a higher-order approximation through virtual spin-flip processes even in the case of $t' = 0$.[74,75] As a result, the dispersion law of the band holes is given by

$$\epsilon_{\mathbf{k}\sigma} = \alpha \gamma_{\mathbf{k}}^2 + \beta \gamma_{2\mathbf{k}}, \quad (30)$$

where $\gamma_{\mathbf{k}}$ is determined by Eq. (14). The prefactors are given by

$$\alpha = 8t' \pm \frac{\delta t^2}{2(2J - t')}, \quad \beta = -2(t' - 2t''), \quad (31)$$

when the propagation of the holes occurs due to the direct hopping (t'' is a hopping term corresponding to third neighbors). They are proportional to J when the propagation is due to the virtual spin-flip processes.[74,75] For realistic values of the parameters, the dispersion law (30) is characterized by minima located at the four points $(\pm\pi/2, \pm\pi/2)$.[73]

C. Fermi surfaces for different solutions

Let us analyze now the shape of the FS corresponding to different solutions for the normal state. The shape of the Fermi surface of the doped holes on the AF background characterized by the dispersion law (30) is well known. It is represented by four small pockets around the points $(\pm\pi/2, \pm\pi/2)$; see Fig. 1. The volume of the Fermi surface is proportional to the number of doped holes δ.

For the state without LR ordering (paramagnetic phase), the FS of the quasiparticles with the dispersion law (17) depends crucially on the value of chemical potential. The latter is determined by solutions of Eq. (26). One can see that at

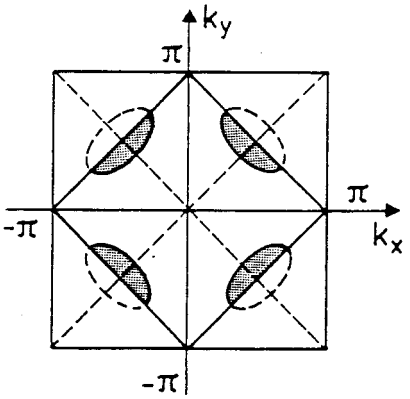

FIG. 1. Fermi surface of carriers in the AF state I′.

$T=0$ Eq. (25) for the chemical potential has two solutions for each δ: $\mu<0$ (solution I) and $\mu>0$ (solution II) (since at $T=0$ one has $m=1$ for $\mu>0$ and $m=0$ for $\mu<0$). Solution I is described by the equation

$$\delta=\frac{1}{N}\sum_{k\sigma} n^F(\epsilon_{\mathbf{k}\sigma}-\mu) \tag{32}$$

and solution II by the equation

$$1+\delta=\frac{1}{N}\sum_{k\sigma} n^F(\epsilon_{\mathbf{k}\sigma}-\mu), \tag{33}$$

where $\epsilon_{\mathbf{k}\sigma}$ is determined by Eq. (17). [To get these equations one should not forget that the sum in Eq. (26) includes a summation on σ so that the last term equals -2 in the case of $\mu>0$.] The corresponding FS's are shown in Fig. 2 for the same value of doping, $\delta=0.1$, and for two cases (i) $t'=0$ and (ii) $t'/t\neq 0$ being negative. The FS is large in case (33) and small in case (32). Another important observation is that the shape of the large FS depends a lot on the ratio of hopping parameters while the shape of the small FS is practically independent.

At finite temperature, the dependence $\mu(\delta)$ is obtained by a numerical solution of Eq. (26). The results for the case $t'=0$ and $t'\neq 0$ are shown in Figs. 3(a) and 3(b) (together with the results for $T=0$). One can see that at very low and very high doping only one solution exists in the case of $T\neq 0$, I and II, respectively, whereas at intermediate doping two solutions coexist. The third solution which corresponds to the parts of curves $\mu(\delta)$ with a negative slope is an unphysical solution (in a direct analogy with the van der Waals equation). For the interval of doping where the three solutions coexist, the physical picture is the following. Within this interval, a critical doping $\delta_0(T)$ exists at which a first-order phase transition from solution I to solution II takes place. This doping is determined by the condition of the equality of the free energies associated with solutions I and II. At very high temperature, however, only one solution persists for any doping [see curves for $T=t$ in Figs. 3(a) and 3(b)]. This means that the line of the first-order PT, $\delta_0(T)$, terminates at some temperature by a critical point. We do not perform explicit calculations of $\delta_0(T)$ since in order to obtain reliable values of the free energies the calculations should be performed in a higher-order approximation (because of the close values of the free energies for these phases). Important itself is the fact of the existence of the first-order phase transition at some intermediate doping.

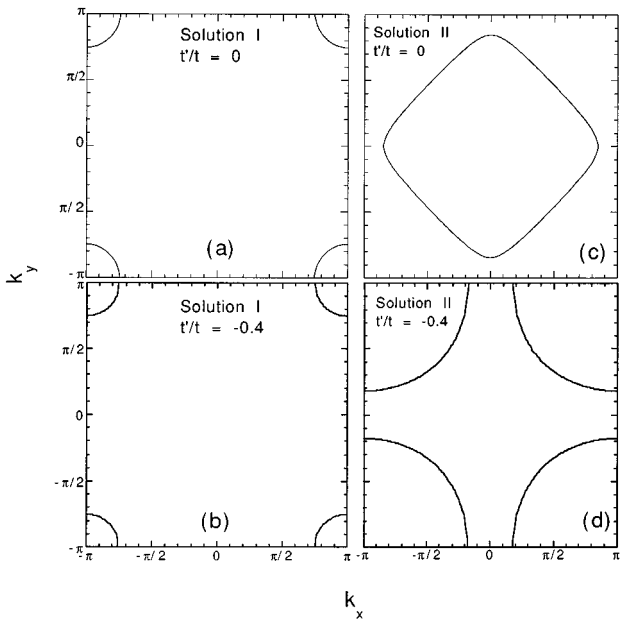

FIG. 2. Hole Fermi surfaces in the PM state. Calculations are performed for the doping level $\delta=0.1$ and two cases of parameters $t/J=1.8$, $t'/t=0$, (a) and (c), and $t/J=1.8$, $t'/t=-0.4$, (b) and (d). The plots (a) and (b) correspond to solution I, the plots (c) and (d) to solution II.

To understand the nature of the states described by solutions I and II let us analyze the behavior of the spin Green function corresponding to these solutions. As seen from Eq. (23), the spin Green function exhibits an AF instability as the temperature decreases in the case of solution I but does not in the case of solution II. It is so because $C(T)$ is finite as $T\rightarrow 0$ for solution I but $C(T)\rightarrow 0$ [and moreover $C(T)/T\rightarrow 0$] as $T\rightarrow 0$ for solution II; see Eq. (22). It means that the paramagnetic solution I is unstable against AF ordering when lowering the temperature. On the contrary, solution II is stable against LR AF ordering as T decreases, and the metallic PM state described by solution II exists at $T=0$ as well.[76]

Hence, the two discussed solutions correspond to qualitatively different physical pictures. In the case of solution I, the FS is formed by only doped holes whereas holes on copper are responsible for localized magnetism. In the case of solution II, holes on copper become a part of the FS while the system loses the localized magnetic moments associated with d electrons.

Thus, what happens can be described as follows. At ''high'' temperature and low doping, only one PM solution exists, namely, solution I with a small FS. This solution, however, is unstable against AF ordering when lowering the temperature so far as the spin susceptibility diverges at $\mathbf{k}=\mathbf{Q}_{\mathrm{AF}}$. Therefore, at low temperature and low doping, instead of solution I the AF solution (which we will call I′) is realized, and the hole dynamics is described by the hole Green function (A18) and (A19). [Strictly speaking, for this solution the long-range AF order takes place only at $T=0$ for

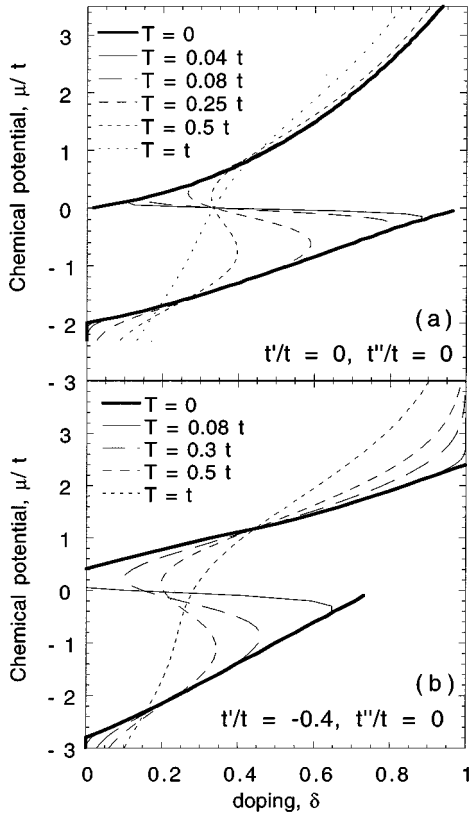

FIG. 3. Doping dependence of chemical potential obtained by the solution of Eq. (26) for two cases of parameters $t'/t=0$ and $t'/t=-0.3$. The parts of the curves with $\mu<0$ correspond to solution I while those with $\mu>0$ correspond to solution II. The parts of the curves with a negative slope correspond to an unphysical solution (in direct analogy with the van der Waals equation).

the two-dimensional (2D) CuO_2 plane. Actually, however, an exchange interaction between planes is always present, leading to the stability of LR AF order at low temperature below $T_N(\delta)$.] Accordingly, the FS has the shape shown in Fig. 1. In its turn, the AF ground state becomes unstable above the rather low critical concentration, $\delta=\delta_N^{2D}\approx 0.02-0.03$; see Ref. 69 in which the spin dynamics corresponding to the solution I′ is analyzed in detail. The reason for the instability is the following: Due to the scattering by band holes with the dispersion law (30), magnons with wave vectors close to Q_{AF} lose their identity and decay into electron-hole pairs.[69] Above this concentration but below $\delta_0(0)$, i.e., at $\delta_N^{2D}<\delta<\delta_0$, the only possibility that exists is a quantum spin-liquid or quantum-disordered ground state[77] (another type of ground state associated with the localized-spin system with an AF interaction). At doping levels higher than δ_0, the system exists in the metallic ground state described by solution II. For this solution, the FS is large even at small values of δ; see Fig. 2.

Summarizing, at $\delta=\delta_0$ the low-temperature hole and spin dynamics change abruptly: from the picture of FS formation by doped holes only while *d*-electrons are responsible for the localized magnetism, to the picture when the *d* electrons become a part of the FS while the system loses the magnetic moments associated with *d* electrons. Accordingly the shape and volume of the FS change abruptly from a small FS with a volume proportional to δ to a large FS with a volume proportional to $1+\delta$. In the same way a number of carriers changes.

D. Saddle-point singularity in the case of the large FS

Let us consider now in more details the hole dynamics corresponding to solution II with a large FS. As we will see later on, just the state corresponding to this solution reveals the features close to experimental observations in the normal state at doping levels corresponding to optimal superconductivity and, moreover, the itinerant quasiparticles of this solution have a tendency of SC pairing of high amplitude when lowering T.

As we have already seen, the shape of the large FS at fixed doping depends strongly on the ratio of hopping parameters t'/t. On the other hand, it depends on doping. In Fig. 4 we show a doping evolution of the FS for three sets of t'/t.

The first point, a sensibility of the shape of the FS to the value of t'/t, has already been discussed in the literature in connection with different shapes of the FS for $La_{2-x}Sr_xCuO_4$ (LSCO) and YBCO families obtained by local-density-approximation (LDA) calculations and ARPES experiments. LDA calculations[78–80] reveal that for the family of bilayer cuprates the FS shape is rotated by 45° relative to that found in a nearest-neighbor tight-binding scheme. By contrast, the same calculations show that for the LSCO family the FS has a diamondlike shape. Thus, two families of cuprates have FS's which roughly speaking are related by 45° rotation. The experiments confirm this, directly by ARPES measurements[13–20] for bilayer cuprates and indirectly by neutron scattering measurements for LSCO; the latter reveal the existence of nested FS.[81] The idea of fitting these shapes by using different values of the ratio t'/t for these compounds, large and negative for YBCO and small for LSCO, has appeared in many papers; see, for example, Refs. 82 and 83. Below we choose the ratio $t'/t=-0.1$ to model the LSCO family and we analyze a few possibilities, including $t'/t=-0.3$ and $t'/t=-0.4$, for the YBCO family.

The second point which we would like to discuss in more detail is the evolution of FS with doping and the related features of the dispersion law of the itinerant quasiparticles. In Fig. 5 we show the dispersion law $\epsilon_{\mathbf{k}\sigma}$ given by Eq. (17) in the directions (1,0) and $(\pi,1)$ for the parameters $t'/t=-0.1$ (to model the LSCO family) and $t'/t=-0.3$ and $t'/t=-0.4$ (to be analyzed for the YBCO family). (We remind the reader that $\epsilon_{\mathbf{k}\sigma}$ is written in the hole representation.)

The dispersions are similar to those in the band calculations, but differ by the multiplier $(1+\delta)/2$. The latter is important since it accounts for experimentally observed narrowing of the bandwidth by a factor of 2 in comparison with band theory, as first noted by the Olson's group.[84]

The dispersion is characterized by saddle points (SP's) located at $(\pm\pi,0)$ and $(0,\pm\pi)$ with the energy

$$\epsilon_s=-2(1+\delta)t'. \tag{34}$$

Near the saddle points, the dispersion law can be written as

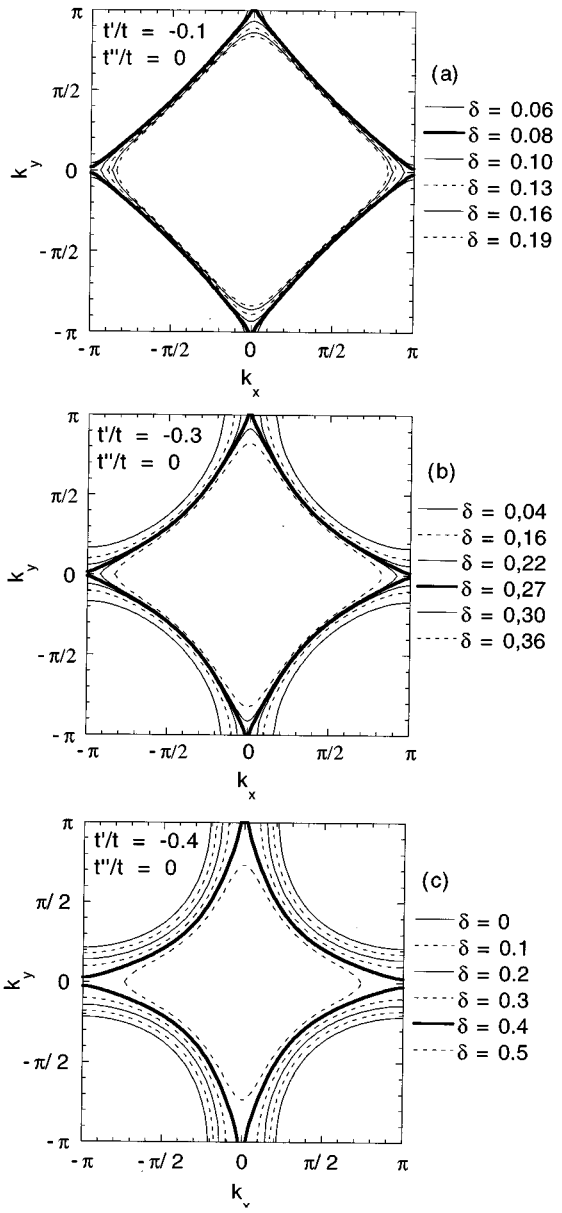

FIG. 4. Evolution of the FS with doping in the case of solution II for different sets of parameters.

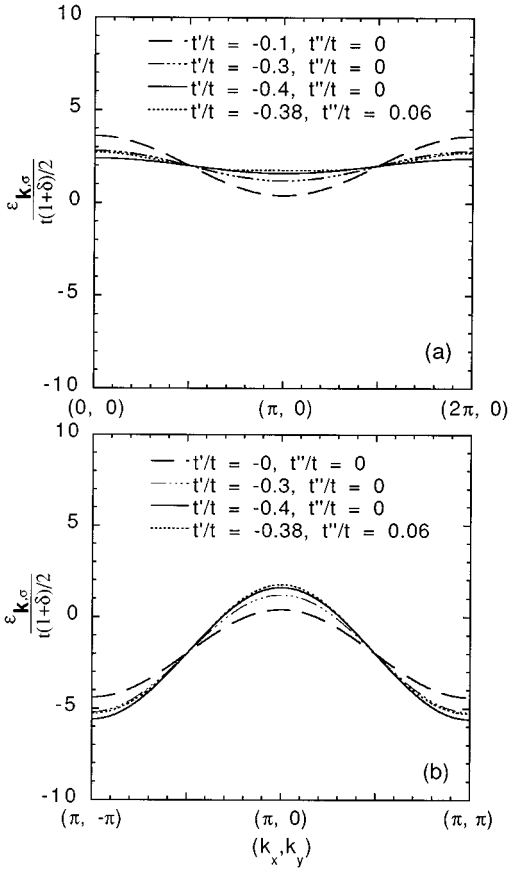

FIG. 5. Hole dispersion law corresponding to solution II in the directions (1,0) and $(\pi,1)$ for three sets of hopping parameters. Note that the dimensionless spectrum plotted, $\epsilon_{\mathbf{k}\sigma}/\ t[(1+\delta)/2]=2(\cos k_x+\cos k_y)+4t'/t\cos k_x\cos k_y+2t''/t(\cos 2k_x+\cos 2k_y)$, is also doping independent. The true spectrum depends on doping by a factor of $(1+\delta)/2$.

$$\frac{\epsilon_{\mathbf{k}\sigma}}{(1+\delta)/2}=-4t'+k_\alpha^2(t+2t')-k_\beta^2(t-2t'), \qquad (35)$$

where $\alpha=x,\beta=y$ for the points $(\pm\pi,0)$ and $\alpha=y,\beta=x$ for the points $(0,\pm\pi)$. For $t'\neq 0$ this dispersion law is characterized by a heavy mass, $m_1\propto 1/(t-2|t'|)$, in one direction and by a light mass, $m_2\propto 1/(t+2|t'|)$, in the other. As a result for large enough $|t'/t|$, the spectrum around the saddle points is characterized by a flat minimum along the Y-Γ direction and by a narrow maximum along the Y-S direction (in the hole representation). Such a behavior is very close to that observed by ARPES in different bilayer high-T_c oxides $YBa_2Cu_3O_{6+x}$ (YBCO123), $YBa_2Cu_4O_8$ (YBCO124), and $Bi_2Sr_2Ca_1Cu_2O_6$ (Bi2212).[10–20] However, the experimentally observed extension of the flat part in the Y-Γ direction is larger than the calculated one seen in Fig. 5. To reproduce the experimental dispersion curve better[85] one can add a next-next-nearest-neighbor hopping term t'' to force a k_α^4 dependence into the dispersion law.[86] The spectrum $\epsilon_{\mathbf{k}\sigma}$ for this case is also shown in Fig. 5 for the values of hopping parameters proposed in Ref. 86. (In the following section we will analyze all sets of parameters in a relation with superconductivity phenomenon.)

The important question is how far is the energy of the SP from the Fermi level and how the distance between them changes with doping? In Fig. 6 we show two curves $\epsilon_F(\delta)$ calculated self-consistently based on Eq. (26) and $\epsilon_s(\delta)$ from Eq. (34) for the cases $t'/t=-0.1$ and $t'/t=-0.3$. One can see that at some critical doping $\delta=\delta_c$, two curves intersect. For the case $t'/t=-0.1$ (monolayer cuprates) one has $\delta_c\approx 0.08$, and for the case $t'/t=-0.3$ (bilayer cuprates) one has $\delta_c\approx 0.27$. For the doping range $\delta<\delta_c$, the Fermi level lies below the saddle-point energy (or above in the electron representation), being very close to it. The fact that the difference $Z=|\epsilon_F-\epsilon_s|$ is small and changes only little within the extended range of doping for $\delta<\delta_c$ for the case of the bilayer cuprates is very important, for it allows one to understand the experimental observation for the bilayer compounds in the underdoped regime.[88] In correspondence to these observations, the distance between the saddle point and the Fermi level is smaller than 30 meV for all doping in the

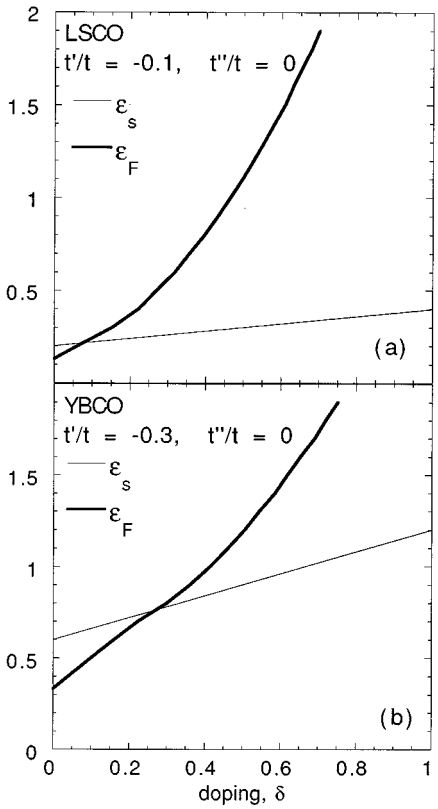

FIG. 6. Energies of the saddle point and of the Fermi level as functions of doping for parameters which model the monolayer and bilayer cuprates.

underdoped regime. This observation cannot be understood within band calculations, as emphasized in Ref. 88. On the contrary, as seen from Fig. 6(b), our calculations give $Z<0.14t=0.25J\approx 30$ meV for the doping range $\delta=0.1-0.4$.[89]

The weak variation of $|\epsilon_F-\epsilon_s|$ with doping in the underdoped regime, i.e., at $\delta<\delta_c$, results in a weak change of the FS within the extended doping range from low doping to the critical one, $\delta=\delta_c$; see Fig. 4. Such a weak change is also in good agreement with the photoemission experiment; see Ref. 11.

The intersection of two curves $\epsilon_F(\delta)$ and $\epsilon_s(\delta)$ has important effects on the normal-state hole dynamics. The first is the known zero-energy logarithmic singularity in the density of states (see, for example, Ref. 13),

$$\rho(\omega)=\sum_{\mathbf{k}\sigma}\delta(\omega-\epsilon_{\mathbf{k}\sigma}-\mu)\sim\ln|\omega-Z|, \tag{36}$$

occurring at $Z=0$ where Z is the distance from the critical doping, $Z=\epsilon_s-\epsilon_F\sim\delta_c-\delta$ when δ tends to δ_c. This singularity has an important influence on the thermodynamic properties. The second is the non-Fermi-liquid, $\omega\ln\omega$, behavior of the inverse relaxation time related to electron-electron scattering occurring at $Z=0$ which transforms to usual Fermi-liquid behavior far from $\delta=\delta_c$:[87,93,94]

$$\tau_{e-e}^{-1}(\omega)=\begin{cases}\omega\ \ln|\omega-Z|, & \omega-Z\ll T,\\ \omega^2\ln|\omega-Z|, & \omega-Z\gg T, \quad Z<0.\end{cases} \tag{37}$$

There is also a singular behavior of the inverse relaxation time related to impurity scattering which occurs as well at $Z=0$, $\tau_{\mathrm{imp}}^{-1}(\omega)\sim\ln\omega$ for $T\gg\omega$.[87] (We would like to emphasize again that the intersection of the SP and FL discussed above is not assumed but is obtained self-consistently.)

In total, anomalies which occur at $\delta=\delta_c$ are signatures of quantum critical behavior related to an electronic topological transition (ETT) in the system of noninteracting carriers. A general theory of such transitions related to the change in the topology of FS's is discussed in Ref. 96. Applications for 3D systems are considered in Ref. 97. On our opinion, just the proximity of the system to the quantum critical point related to the ETT in the quasi-2D case of cuprates is responsible for the so-called ''strange metal'' behavior observed in the normal state above T_c. The details of such critical behavior occurring in the system of interacting carriers are discussed elsewhere.[87]

Summarizing, solution II which describes the normal-state hole dynamics in the intermediate doping exhibits features quite close to those observed experimentally. We would like to emphasize that this starting picture of the hole dynamics in the normal state is quite different from that obtained in two types of microscopical theories based on the t-J model; see Refs. 6–8, 98 and 99. In Refs. 6–8 the normal-state hole dynamics coincides with the picture corresponding to solution I′ (in our notation). In Refs. 98 and 99, the normal-state hole dynamics corresponds to solution I. Both pictures are very different from that found in the present paper and from the picture observed experimentally.

Let us consider now the possibility of a superconducting pairing of the discussed quasiparticles characterized by the dispersion laws shown in Fig. 5 and by the FS shown in Fig. 4.

IV. SUPERCONDUCTING PAIRING

A. Direct attractive interaction between carriers in the t-J model

The quasiparticles which we have discussed in Secs. II and III are, on the one hand, close to the usual fermions so far as they are characterized by FS's, etc. On the other hand, by kinematic properties they belong to the family of the lieons (see Sec. II) and this results in various specific consequences. The most important for us here is the point that due to this specificity of the quasiparticles, the hopping term of the Hamiltonian and the exchange interaction turn out to be direct attractive interactions between them.

To understand this effect, it is necessary to comprehend the nature of vertex blocks representing a Lie-Hubbard operator X_i^{pq} which are different from the vertex blocks for Bose and Fermi operators due to the intrinsic differences in the algebras. (The graphs discussed below correspond to the DT for LH operators. To understand the details we address the reader to Ref. 57, Appendix B.) We show some vertices representing the spin-flip operator $X_i^{\sigma\sigma'}$ and the charged-quasiparticle operator $X_i^{0\sigma}$ in Figs. 7 and 8, respectively. The crucial point demonstrated by the figures is that in contrast to the DT for Bose or Fermi operators, the LH operator X_i^{pq} can be represented not only by simple vertex blocks to (or from) which one Green-function line comes in [Figs. 7(a) and 8(a)]

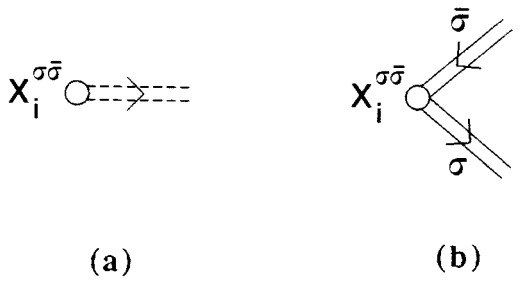

FIG. 7. Vertex blocks corresponding to the spin-flip LH operator $X_i^{\sigma\bar{\sigma}}$. Here and later on we keep for the graph elements the same notations as in Ref. 57: The double solid line corresponds to the hole Green function K^h defined by Eq. (16), the double dashed line to a propagator-type spin Green function K^S. The system of pairing of operators by the Wick theorem corresponding to graph (a) is given by $\langle T_\tau X_i^{\sigma\bar{\sigma}}(\tau) X_1^{\bar{\sigma}\sigma}(\tau_1)\rangle_0 = K^S(\tau-\tau_1)\langle X_1^{\sigma\sigma} - X_1^{\bar{\sigma}\bar{\sigma}}\rangle_0$ and to graph (b) by $\langle T_\tau X_1^{\bar{\sigma}0}(\tau_1) X_i^{\sigma\bar{\sigma}}(\tau) X_2^{0\sigma}(\tau_2)\rangle_0 = -K^h_{\bar{\sigma}\bar{\sigma}}(\tau_1-\tau)K^h_{\sigma\sigma}(\tau-\tau_2)\langle X_2^{00} + X_2^{\sigma\sigma}\rangle_0$. Graph (a) corresponds to a direct spin flip, graph (b) to the spin flip associated with the creation of one carrier with spin σ and the annihilation of the other with spin $\bar{\sigma}$.

but also by complex vertex blocks in which several Green functions meet (without any interaction line) [Figs. 7(b), 8(b), and 8(c)]. In other words, each LH operator carries an interaction (an anharmonicity) in itself. Mathematically this is a consequence of their specific algebra, namely, of the multiplication rules (6) and commutation relations (7). Due to these commutation relations, two LH operators after pairing in correspondence to the Wick theorem give again a LH operator in contrast to Bose-Fermi operators which give after pairing 1 or 0. Hence, after a first pairing, another LH operator can participate in a second pairing with the initial LH operator, then again new operator can, and so on. This is the way in which the complex blocks appear. In more detail with some examples we have discussed this procedure in Ref. 57, Appendix B.

It should be emphasized again that the existence of such complex blocks is intrinsic and it stems from the algebra of X operators; the structure of the complex blocks depends neither on the type of Hamiltonian or on the approximation in which the latter is treated. Thus, the types of complex vertex blocks come from the algebra; however, the type of graph in which these blocks participate depends on the Hamiltonian. Each interaction $V_{ij}X_i^{pq}X_j^{p'q'}$ produces a line (wavy line in the graphs) which joins a vertex block corresponding to the operator X_i^{pq} with a vertex block corresponding to the operator $X_j^{p'q'}$; see for example Figs. 9–13. [To read the graphs one has to remember that their elements have a different meaning than those in the DT for Fermi-Bose operators. Namely, here the interaction lines are very important and they are shown by wavy lines not by a simple crossing of Green-function lines. A simple crossing of the Green-function lines corresponds to some LH operator (shown as an open circle).]

One can see now that the same interaction V_{ij}, given by the Hamiltonian $V_{ij}X_i^{pq}X_j^{p'q'}$, plays a different role when it joins different types of vertex blocks corresponding to the operators X_i^{pq} and $X_j^{p'q'}$. Namely, in the considered case of the t-J model, the Hamiltonian H_J plays the role of an exchange interaction between the localized spins when the $J_{\mathbf{k}}$ line joins two vertex blocks of type (a) in Fig. 7 and the role of an interaction between two charged quasiparticles when the $J_{\mathbf{k}}$ line joins two blocks of type (b) in Fig. 7 as shown in Fig. 9. H_t plays the role of the propagation energy of carriers when the $t_{\mathbf{k}}$ line joins two blocks of type (a) in Fig. 8 and the role of an interaction between two charged quasiparticles when it joins the vertex block of type (a) with that of type (c) in Fig. 8 as shown in Fig. 9.

Thus, skeleton diagrams responsible for the interactions which can lead to SC pairing of charged quasiparticles are the graphs shown in Fig. 9.[100] Being dependent on wave vectors, these interactions are attractive in some regions of the Brillouin zone and repulsive in others. (The possibility of

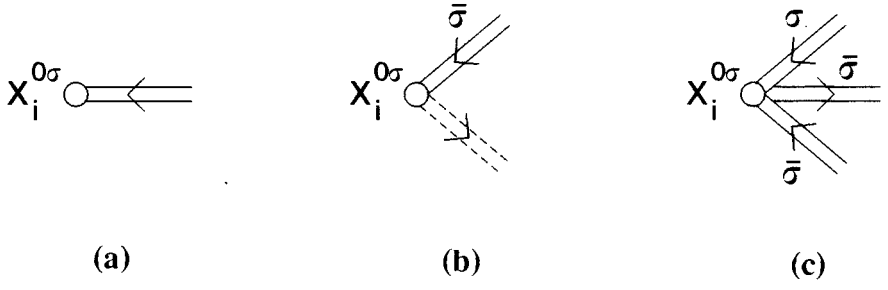

FIG. 8. Vertex blocks corresponding to the operator $X_i^{0\sigma}$ associated with the carrier creation. The system of pairing corresponding to graph (a) is given by $\langle T_\tau X_1^{\sigma 0}(\tau_1) X_i^{0\sigma}(\tau)\rangle_0 = K^h_{\sigma\sigma}(\tau_1-\tau)\langle X_i^{00} + X_i^{\sigma\sigma}\rangle_0$, to graph (b) by $\langle T_\tau X_1^{\bar{\sigma}0}(\tau_1) X_i^{0\sigma}(\tau) X_2^{\sigma\bar{\sigma}}(\tau_2)\rangle_0 = K^h_{\bar{\sigma}\bar{\sigma}}(\tau_1-\tau)K^S(\tau-\tau_2)\langle X_2^{\bar{\sigma}\bar{\sigma}} - X_2^{\sigma\sigma}\rangle_0$, and to graph (c) by $\langle T_\tau X_1^{\sigma 0}(\tau_1) X_i^{0\sigma}(\tau) X_2^{\bar{\sigma}0}(\tau_2) X_3^{0\bar{\sigma}}(\tau_3)\rangle_0 = K^h_{\sigma\sigma}(\tau_1-\tau)K^h_{\bar{\sigma}\bar{\sigma}}(\tau_2-\tau)K^h_{\bar{\sigma}\bar{\sigma}}(\tau-\tau_3)\langle X_3^{\bar{\sigma}\bar{\sigma}} + X_3^{00}\rangle_0$. Graph (a) corresponds to a direct creation of carrier, graphs (b) and (c) to higher-order processes through intermediate quasiparticles.

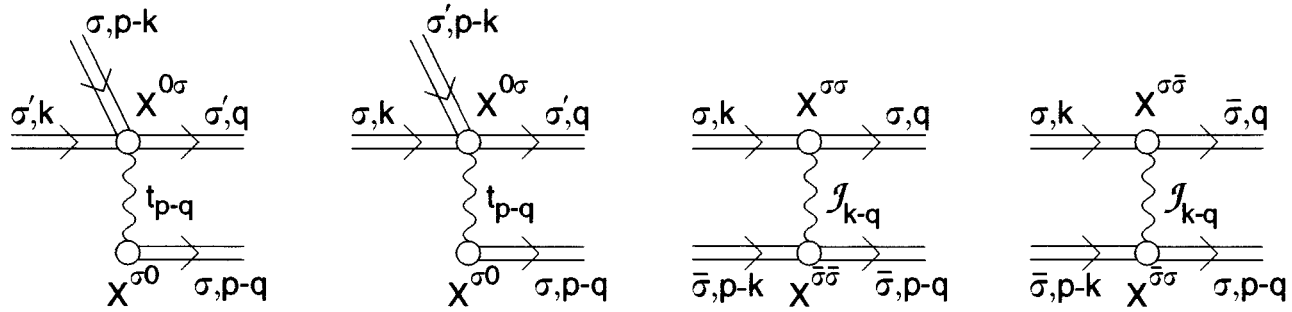

FIG. 9. Graphs showing the origin of the attractive interaction between carriers.

an attraction between carriers due to a hopping term was discussed early in Ref. 101 for the Hubbard model.)

In order to feel the physical meaning, it is useful to recall the situation for the more simple (and more known) case of operators belonging to the LH family, spin operators. Indeed, for the case of spin operators a similar effect is well known. It appears in different formalisms. For example, in the Dyson-Maleev representation for spin operators, a nondiagonal spin operator is written as the sum of the linear and third-order terms on Bose operators so that the same exchange interaction produces an energy of spin waves and their interaction. In another formalism, the DT for spin operators, the same effect manifests itself as the simultaneous existence of the simple vertex block with one Green-function line and of the complex vertex block with three Green-function lines, both representing the same operator S_i^+ (see Ref. 56).

The existence of the interactions shown in Fig. 9 allows us to write down an equation for the anomalous hole Green function,

$$G^h_{\sigma\bar{\sigma}}(\mathbf{k},i\omega_n)=\langle\langle X^{\sigma 0}_{\mathbf{k}} X^{\bar{\sigma}0}_{-\mathbf{k}}\rangle\rangle = \int_{-\beta}^{\beta} d\tau\, \exp(-i\omega_n\tau)\langle T_\tau X^{\sigma 0}_{\mathbf{k}}(\tau) X^{\bar{\sigma}0}_{\mathbf{k}}(0)\rangle, \tag{38}$$

associated with a SC pairing of carriers. As usual in the DT for X operators, in fact the graphical equation concern to the Fermi-type anomalous hole Green function $K^h_{\sigma\bar{\sigma}}$ related to the true Green function $G^h_{\sigma\bar{\sigma}}$ in the same way as it was in the case of the normal hole Green function [see Eq. (16) and Ref. 70], namely, by the relation

$$G^h_{\sigma\bar{\sigma}}=b^{\sigma 0}K^h_{\sigma\bar{\sigma}}. \tag{39}$$

Such an equation is given by

$$\begin{aligned}\widetilde{K}^h_{\sigma\bar{\sigma}}&=(K^h_{\sigma\sigma}\Pi_{\sigma\bar{\sigma}}K^h_{\bar{\sigma}\bar{\sigma}}+K^h_{\sigma\sigma}\Pi_{\sigma\bar{\sigma}}K^h_{\bar{\sigma}\bar{\sigma}}\Pi_{\bar{\sigma}\bar{\sigma}}K^h_{\bar{\sigma}\bar{\sigma}}+\cdots)\\&\quad+(K^h_{\sigma\sigma}\Pi_{\sigma\sigma}K^h_{\sigma\sigma}\Pi_{\sigma\bar{\sigma}}K^h_{\bar{\sigma}\bar{\sigma}}+\cdots)\\&=K^h_{\sigma\sigma}\Pi_{\sigma\bar{\sigma}}\widetilde{K}^h_{\bar{\sigma}\bar{\sigma}}+K^h_{\sigma\sigma}\Pi_{\sigma\sigma}\widetilde{K}^h_{\sigma\bar{\sigma}},\end{aligned} \tag{40}$$

where $\widetilde{K}^h_{\sigma\sigma}$ is given by

$$\begin{aligned}\widetilde{K}^h_{\sigma\sigma}&=K^h_{\sigma\sigma}+(K^h_{\sigma\sigma}\Pi_{\sigma\sigma}K^h_{\sigma\sigma}+K^h_{\sigma\sigma}\Pi_{\sigma\sigma}K^h_{\sigma\sigma}\Pi_{\sigma\sigma}K^h_{\sigma\sigma}+\cdots)\\&\quad+(K^h_{\sigma\sigma}\Pi_{\sigma\bar{\sigma}}K^h_{\bar{\sigma}\bar{\sigma}}\Pi_{\bar{\sigma}\sigma}K^h_{\sigma\sigma}+\cdots)=K^h_{\sigma\sigma}\\&\quad+K^h_{\sigma\sigma}\Pi_{\sigma\sigma}\widetilde{K}^h_{\sigma\sigma}+K^h_{\sigma\sigma}\Pi_{\sigma\bar{\sigma}}\widetilde{K}^h_{\bar{\sigma}\sigma}.\end{aligned} \tag{41}$$

In Eqs. (40) and (41), $\widetilde{K}^h_{\bar{\sigma}\sigma}$ is an anomalous Green function, $\widetilde{K}^h_{\sigma\sigma}$ is a renormalized normal Green function, $K^h_{\sigma\sigma}$ is the bare normal Green function determined by Eq. (16), and $\Pi_{\sigma\sigma}$ and $\Pi_{\sigma\bar{\sigma}}$ are normal and anomalous components of polarization operator.

In the lowest approximation (first approximation with respect to $1/z$) the latter are given by the graphs in Figs. 10 and 11 taken without external Green-function lines and with internal lines corresponding to the ''dressed'' Green functions $\widetilde{K}^h_{\sigma\sigma}$ and $\widetilde{K}^h_{\bar{\sigma}\sigma}$.[102] The analytical expressions corresponding to these graphs are given by

$$\Pi_{\sigma\bar{\sigma}}(\mathbf{k})=-\frac{1}{N}\sum_{\mathbf{q}} 2(J_{\mathbf{k}-\mathbf{q}}-t_{\mathbf{q}})F_{\mathbf{q}}, \tag{42}$$

$$\Pi_{\sigma\sigma}(\mathbf{k})=-\frac{1}{N}\sum_{\mathbf{q}} (2J_{\mathbf{0}}+J_{\mathbf{k}-\mathbf{q}}-2t_{\mathbf{k}}-2t_{\mathbf{q}})N_{\mathbf{q}}, \tag{43}$$

where the normal and anomalous correlation functions $N_{\mathbf{q}}$ and $F_{\mathbf{q}}$ are related to the normal and anomalous Green functions by

$$N_{\mathbf{q}}=\lim_{\tau\to 0^-}\sum_{\omega_n} G^h_{\sigma\sigma}(\mathbf{q},\omega_n)e^{i\omega_n\tau}, \tag{44}$$

$$F_{\mathbf{q}}=\lim_{\tau\to 0^-}\sum_{\omega_n} G^h_{\sigma\bar{\sigma}}(\mathbf{q},\omega_n)e^{i\omega_n\tau}. \tag{45}$$

In other words, $N_{\mathbf{q}}$ and $F_{\mathbf{q}}$ are normal and superconducting order parameters (OP's) which are Fourier transforms of following ones in real space:

$$F_\eta=\langle X^{\sigma 0}_i X^{\bar{\sigma}0}_{i+\eta}-X^{\bar{\sigma}0}_i X^{\sigma 0}_{i+\eta}\rangle, \tag{46}$$

$$N_\eta=\langle X^{\sigma 0}_i X^{0\sigma}_{i+\eta}\rangle. \tag{47}$$

We omit in Eq. (42) the term corresponding to the last graph in Fig. 10 since it vanishes due to the constraint

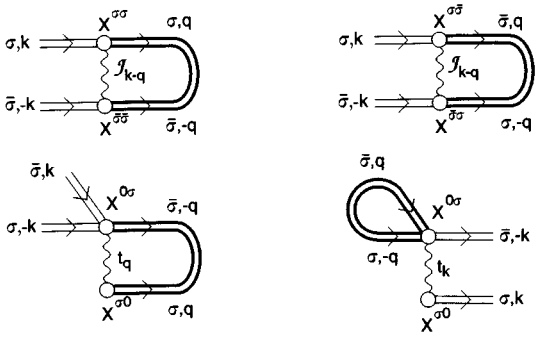

FIG. 10. Graphs originated from vertex blocks in Fig. 9 and contributing to the anomalous component of the polarization operator $\Pi_{\sigma\bar{\sigma}}$. The latter is given by the graphs taken without external Green-function lines.

$$\sum_{\mathbf{p}} F_{\mathbf{p}} = 2 \sum_{i} X_i^{\sigma 0} X_i^{\bar{\sigma} 0} = 0, \tag{48}$$

resulting from the multiplication rules for LH operators:

$$X_i^{\sigma 0} X_i^{\bar{\sigma} 0} = 0. \tag{49}$$

By solving Eqs. (40) and (41) one obtains for the normal and anomalous hole Green functions:

$$\tilde{G}^h_{\sigma\sigma}(\mathbf{k}, i\omega_n) = b^{\sigma 0}\left(\frac{U_{\mathbf{k}}^2}{E_{\mathbf{k}\sigma} - i\omega_n} + \frac{V_{\mathbf{k}}^2}{E_{\mathbf{k}\sigma} + i\omega_n}\right), \tag{50}$$

$$\tilde{G}^h_{\sigma\bar{\sigma}}(\mathbf{k}, i\omega_n) = -b^{\sigma 0} U_{\mathbf{k}} V_{\mathbf{k}}\left(\frac{1}{E_{\mathbf{k}\sigma} - i\omega_n} + \frac{1}{E_{\mathbf{k}\sigma} + i\omega_n}\right), \tag{51}$$

where

$$E_{\mathbf{k}\sigma} = \sqrt{\tilde{\epsilon}_{\mathbf{k}\sigma}^2 + \Delta_{\mathbf{k}}^2}, \tag{52}$$

$$\tilde{\epsilon}_{\mathbf{k}\sigma} = \epsilon_{\mathbf{k}\sigma} - \Pi_{\sigma\sigma}(\mathbf{k}) - \mu, \quad \Delta_{\mathbf{k}} = -\Pi_{\sigma\bar{\sigma}}(\mathbf{k}), \tag{53}$$

$$U_{\mathbf{k}}^2 = \frac{1}{2}\left(1 + \frac{\tilde{\epsilon}_{\mathbf{k}}}{E_{\mathbf{k}\sigma}}\right), \quad V_{\mathbf{k}}^2 = \frac{1}{2}\left(1 - \frac{\tilde{\epsilon}_{\mathbf{k}}}{E_{\mathbf{k}\sigma}}\right). \tag{54}$$

In Eqs. (50)–(54), $E_{\mathbf{k}\sigma}$ is the dispersion law of carriers in the SC state, $\epsilon_{\mathbf{k}\sigma}$ is the dispersion law in the normal state [defined by Eq. (16) with the additional term related to next-next-nearest hopping, $2t''(\cos 2k_x + \cos 2k_y)$], $\Delta_{\mathbf{k}}$ is the SC gap, and $\Pi_{\bar{\sigma}\sigma}(\mathbf{k})$ and $\Pi_{\sigma\sigma}(\mathbf{k})$ are determined by Eqs. (42) and (43).

So far as the polarization operators entering in (50) and (51) are written in terms of the order parameters $F_{\mathbf{k}}$ and $N_{\mathbf{k}}$ determined in their turn by the Green functions (50) and (51), the latter equations are the equations for the functions $F_{\mathbf{k}}$ and $N_{\mathbf{k}}$ to be solved self-consistently. We will neglect below the renormalization of the normal-state dispersion law and take $\tilde{\epsilon}_{\mathbf{k}\sigma} = \epsilon_{\mathbf{k}\sigma} - \mu$, so far as we have used in the dispersion law $\epsilon_{\mathbf{k}\sigma}$ the effective values of hopping parameters taken to fit the experimental dispersion law and FS. Within this approximation we get a single equation to be solved self-consistently, namely, the equation for the SC gap,

$$\Delta_{\mathbf{k}} = \frac{1+\delta}{2}\frac{1}{N}\sum_{\mathbf{q}} \frac{J_{\mathbf{k}-\mathbf{q}} - t_{\mathbf{q}}}{E_{\mathbf{q}\sigma}} \Delta_{\mathbf{q}} \tanh\left(\frac{E_{\mathbf{q}\sigma}}{2T}\right), \tag{55}$$

where $E_{\mathbf{k}\sigma}$ is given by

$$E_{\mathbf{k}\sigma} = \sqrt{(\epsilon_{\mathbf{k}\sigma} - \mu)^2 + \Delta_{\mathbf{k}}^2} \tag{56}$$

and the SC gap is related to the SC order parameter $F_{\mathbf{p}}$ as follows:

$$\Delta_{\mathbf{k}} = \sum_{\mathbf{p}} (J_{\mathbf{k}-\mathbf{p}} - t_{\mathbf{p}}) F_{\mathbf{p}}. \tag{57}$$

The latter is given by the equation

$$F_{\mathbf{q}} = (1+\delta) U_{\mathbf{q}} V_{\mathbf{q}} \{1 - 2n^F(E_{\mathbf{q}})\} \tag{58}$$

(we omit here and later on the index σ in the dispersion law $E_{\mathbf{k}\sigma}$).

Before to switch over solving Eq. (55) it is worth emphasizing that the considered graphs for the polarization operator are the simplest possible graphs in the t-J model. Other graphs produced by the same vertex blocks and by the same interaction lines are possible. One type of graph which could lead to SC pairing appears if one assumes the existence of a propagator-type spin Green function. These diagrams are

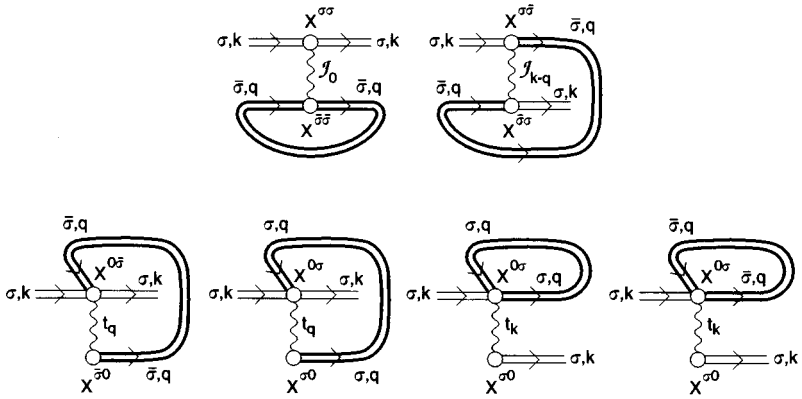

FIG. 11. Graphs which contribute to the normal component of the polarization operator $\Pi_{\sigma\sigma}$. The latter is given by the graphs taken without external Green-function lines.

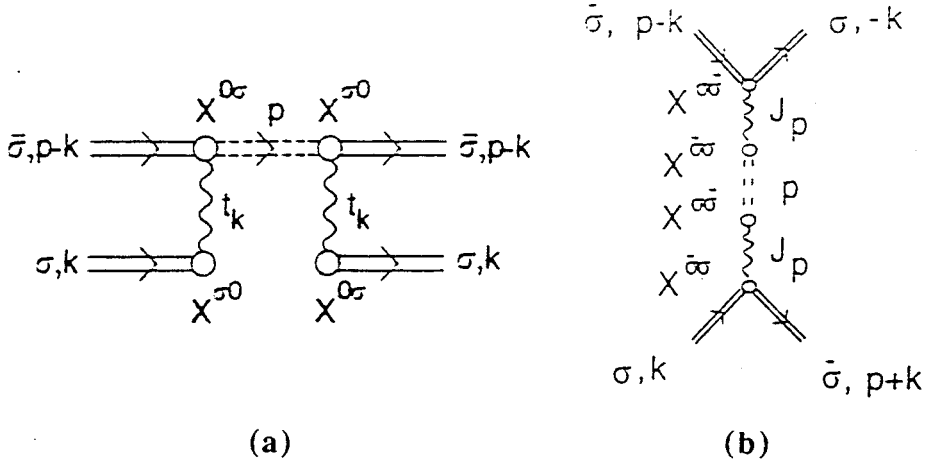

FIG. 12. Graphs for the attractive interaction between carriers appearing through exchange by a virtual magnon.

produced by the skeleton graphs shown in Fig. 12 [the complex vertex blocks participating in the graph 12(a) is of type 8(b) and 8(a) while in the graph 12(b) of type 7(a) and 7(b)]. The graphs in Fig. 12 describe a standard interaction between carriers through an exchange of an intermediate quasiparticle, here by the magnon. Just this type of interaction is usually considered to be responsible for SC pairing of magnetic origin; see, for example, Refs. 6–8. The problem, however, is that vertex blocks of types 8(b) and 7(a), as well as the propagator-type spin Green function itself, nonvanish for zero magnetic field only in the presence of LR AF ordering, which is not the case above T_c. [The reason for the vanishing is the factor $b^{\sigma\sigma}$ (proportional to on-site magnetization) accompanying these vertices and the propagator-type spin Green function. The existence of this factor reflects a general structure of the Green functions determined on LH operators (see Ref. 70)]. Short-range AF correlations, even when strong, do not lead to the appearence of the desired spin Green-function lines.

The latter correlations manifest themselves in another class of diagrams appearing as a result of ''dressing'' of the $J_{\mathbf{k}}$ interaction line as shown in Fig. 13. The corresponding analytical expression for the renormalized J interaction is

$$\widetilde{J}(\mathbf{k},\omega)=\frac{J_{\mathbf{k}}}{1+J_{\mathbf{k}}\chi_0(\mathbf{k},\omega)}\equiv J_{\mathbf{k}}\frac{\chi(\mathbf{k},\omega)}{\chi_0(\mathbf{k},\omega)}, \tag{59}$$

where $\chi_0(\mathbf{k},\omega)$ is a normal-state zeroth susceptibility determined graphically by the loop in Fig. 13 and analytically by the Lindhard function. The effect of such ''dressing'' will be considered elsewhere. As one can see from Eq. (59), in principle, SR AF correlations could lead to an enhancement of the interaction $J_{\mathbf{k}}$, i.e., of the interaction the effect of which on SC pairing is considered in the present paper. We deliberately stay below in the approximation of the bare J interaction since we would like to show that the pure effect of the AF interaction is sufficient to get a high-T_c effect. In other words, we do not want to mix two different effects, the bare attractive interaction existing itself and a possible enhancement coming from SR AF correlations. It is important to distinguish between them in view of the rather popular in phenomenological theories scenario for high-T_c as mediated by SR correlations. On the other hand, the normal-state dynamic spin susceptibility measured by inelastic neutron scattering shows quite smooth behavior as a function of ω,[32,38] which is another argument in favor of considering a bare J interaction.

B. Equation for the superconducting order parameter

The obtained equation (55) for the SC gap is similar to the BCS equation except that it contains the anisotropic interaction potential $J_{\mathbf{k}-\mathbf{q}}-t_{\mathbf{q}}$ in the place of an isotropic one. Recently, such types of anisotropic interactions *have been assumed* in a few phenomenological theories for cuprates (see, for example, Refs. 3–5). A solution of the gap equation has been considered for the case when the dispersion law of carriers and their FS's are taken in the weak-coupling limit (i.e., correspond to those of bare electrons). Although the equations for the SC gap look similarly in our case and in these theories, an important difference exists. In our strong-coupling limit, when the subject for pairing is the quasiparticle associated with the operator $X^{0\sigma}$, the constraint exists given by Eq. (48) which results from the multiplication rules for LH operators. The condition (48) means that the SC OP of these quasiparticles must be sign reversal, with the integral weight of positive and negative parts within the Brillouin zone being equal. This is a strong constraint which forbids, as we will see, many symmetries of the SC OP found in the weak-coupling limit. On the other hand, a formally similar gap equation has been obtained in the strong-

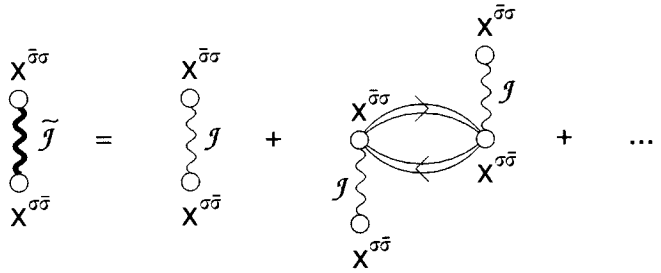

FIG. 13. Graphs for effective exchange interaction ''dressed'' in the presence of SR AF correlations.

coupling limit for the t-J model based on a decoupling scheme for two-time Green functions.[98] However, the normal-state hole dynamics obtained within the decoupling scheme is very different from ours and from that observed experimentally: Namely, it corresponds to solution I in our notation and is characterized by a small FS, as was discussed in Sec. III. Obviously, this changes the explicit solution of the gap equation completely. An additional important difference is a prefactor $(1+\delta)/2$ in the right-hand side of the gap equation which is absent in Ref. 98 and which is important for the doping dependence of the SC gap.

Let us now analyze the equation for the SC gap. Using the explicit momentum dependence of $J_{\mathbf{k}-\mathbf{q}}$ and $t_{\mathbf{k}}$ for a square lattice, one can rewrite Eq. (55) in the following way:

$$\Delta_{\mathbf{k}}=\cos k_x N_x+\cos k_y N_y+\sin k_x M_x+\sin k_y M_y+\Delta, \tag{60}$$

with

$$N_x=\frac{1+\delta}{N}\sum_{\mathbf{q}}\frac{J\cos q_x\Delta_{\mathbf{q}}}{E_{\mathbf{q}}}\tanh\left(\frac{E_{\mathbf{q}}}{2T}\right), \tag{61}$$

$$N_y=\frac{1+\delta}{N}\sum_{\mathbf{q}}\frac{J\cos q_y\Delta_{\mathbf{q}}}{E_{\mathbf{q}}}\tanh\left(\frac{E_{\mathbf{q}}}{2T}\right), \tag{62}$$

$$\Delta=-\frac{1+\delta}{N}\sum_{\mathbf{q}}\frac{2\Delta_{\mathbf{q}}}{E_{\mathbf{q}}}(t\gamma_{\mathbf{k}}+t'\eta_{\mathbf{k}})\tanh\left(\frac{E_{\mathbf{q}}}{2T}\right), \tag{63}$$

and $M_x=M_y=0$, the latter because of symmetry: $\Delta_{\mathbf{k}}=\Delta_{-\mathbf{k}}$. Another (equivalent) presentation of Eq. (60) is

$$\Delta_{\mathbf{k}}=\Delta+\Delta_0^s\gamma_{\mathbf{k}}+\Delta_0^d\alpha_{\mathbf{k}}, \tag{64}$$

in which $\Delta_{\mathbf{k}}$ is represented as a linear combination of a constant term, an extended s-wave symmetry term, and a d-wave symmetry term. In Eqs. (61)–(64), $\alpha_{\mathbf{k}}=\frac{1}{2}(\cos k_x-\cos k_y)$ and $\gamma_{\mathbf{k}}$ and $\eta_{\mathbf{k}}$ are determined by Eq. (14). Substituting Eq. (64) into Eqs. (61)–(63), we obtain a set of coupled equations for the amplitudes of the SC gap, Δ_0^s, Δ_0^d, and Δ:

$$\Delta_0^s=\frac{2J(1+\delta)}{N}\sum_{\mathbf{k}}\left\{\frac{\gamma_{\mathbf{k}}^2\Delta_0^s+\alpha_{\mathbf{k}}\gamma_{\mathbf{k}}\Delta_0^d+\gamma_{\mathbf{k}}\Delta}{E_{\mathbf{k}}}\tanh\left(\frac{E_{\mathbf{k}}}{2T}\right)\right\}, \tag{65}$$

$$\Delta_0^d=\frac{2J(1+\delta)}{N}\sum_{\mathbf{k}}\left\{\frac{\alpha_{\mathbf{k}}^2\Delta_0^d+\alpha_{\mathbf{k}}\gamma_{\mathbf{k}}\Delta_0^s+\alpha_{\mathbf{k}}\Delta}{E_{\mathbf{k}}}\tanh\left(\frac{E_{\mathbf{k}}}{2T}\right)\right\}, \tag{66}$$

$$\Delta=-\frac{t\Delta_0^s}{J}-\frac{2t'(1+\delta)}{N}\times\sum_{\mathbf{k}}\left\{\frac{\eta_{\mathbf{k}}\gamma_{\mathbf{k}}\Delta_0^s+\eta_{\mathbf{k}}\alpha_{\mathbf{k}}\Delta_0^d+\eta_{\mathbf{k}}\Delta}{E_{\mathbf{k}}}\tanh\left(\frac{E_{\mathbf{k}}}{2T}\right)\right\}. \tag{67}$$

In the case of $t'=0$, the system of three equations reduces to a system of two equations while the amplitudes Δ_0^s and Δ are related as follows:

$$\Delta=-\frac{t}{J}\Delta_0^s. \tag{68}$$

Equations (65)–(67) describe a solution of a most general symmetry: $\Delta_0^d\neq 0$, $\Delta_0^s\neq 0$, $\Delta\neq 0$, if it exists. For a particular but most important symmetry, when $\Delta_{\mathbf{k}}^2$ (and so $E_{\mathbf{k}}$) is invariant into the symmetry operation $k_x\leftrightarrow k_y$, the system of equations is reduced to the equation

$$\Delta_0^d=J(B-C)\Delta_0^d \tag{69}$$

and to the set of equations

$$\Delta_0^s=J(B+C)\Delta_0^s+2D\Delta, \tag{70}$$

$$\Delta=-\left(\frac{t}{J}+2t'E\right)\Delta_0^s-2C\Delta, \tag{71}$$

where B, C, D, and E are defined as follows:

$$B=\frac{1+\delta}{N}\sum_{\mathbf{k}}\frac{\cos^2 k_\alpha}{E_{\mathbf{k}}}\tanh\left(\frac{E_{\mathbf{k}}}{2T}\right), \tag{72}$$

$$C=\frac{1+\delta}{N}\sum_{\mathbf{k}}\frac{\cos k_x\cos k_y}{E_{\mathbf{k}}}\tanh\left(\frac{E_{\mathbf{k}}}{2T}\right), \tag{73}$$

$$D=\frac{1+\delta}{N}\sum_{\mathbf{k}}\frac{\cos k_\alpha}{E_{\mathbf{k}}}\tanh\left(\frac{E_{\mathbf{k}}}{2T}\right), \tag{74}$$

$$E=\frac{1+\delta}{N}\sum_{\mathbf{k}}\frac{\cos^2 k_x\cos k_y}{E_{\mathbf{k}}}\tanh\left(\frac{E_{\mathbf{k}}}{2T}\right). \tag{75}$$

This symmetry is consistent with a generalized d-wave symmetry of the SC gap,

$$\Delta_{\mathbf{k}}=\Delta_0^d\alpha_{\mathbf{k}}+\Delta, \tag{76}$$

with a generalized s-wave symmetry

$$\Delta_{\mathbf{k}}=\Delta_0^s\gamma_{\mathbf{k}}+\Delta, \tag{77}$$

and with an $s+id$ symmetry

$$\Delta_{\mathbf{k}}=\Delta+\Delta_0^s\gamma_{\mathbf{k}}+i\Delta_0^d\alpha_{\mathbf{k}}. \tag{78}$$

For these symmetries we finally have a set of three equations, two of which are given by

$$\frac{(1+\delta)}{N}\sum_{\mathbf{k}}\frac{2J\alpha_{\mathbf{k}}^2}{E_{\mathbf{k}}}\tanh\left(\frac{E_{\mathbf{k}}}{2T}\right)=1, \tag{79}$$

$$1=\frac{1+\delta}{N}\left\{\left[\sum_{\mathbf{k}}\frac{2(J\gamma_{\mathbf{k}}^2-t\gamma_{\mathbf{k}})}{E_{\mathbf{k}}}\tanh\left(\frac{E_{\mathbf{k}}}{2T}\right)\right]+\left[\sum_{\mathbf{k}}\frac{4t'\eta_{\mathbf{k}}}{E_{\mathbf{k}}}\tanh\left(\frac{E_{\mathbf{k}}}{2T}\right)\right]\left[\sum_{\mathbf{k}}\frac{J\gamma_{\mathbf{k}}^2}{E_{\mathbf{k}}}\tanh\left(\frac{E_{\mathbf{k}}}{2T}\right)-1\right]-\left[\sum_{\mathbf{k}}\frac{8J\gamma_{\mathbf{k}}}{E_{\mathbf{k}}}\tanh\left(\frac{E_{\mathbf{k}}}{2T}\right)\right]\left[\sum_{\mathbf{k}}\frac{t'\eta_{\mathbf{k}}\gamma_{\mathbf{k}}}{E_{\mathbf{k}}}\tanh\left(\frac{E_{\mathbf{k}}}{2T}\right)\right]\right\}, \tag{80}$$

and the third one has to be chosen among Eqs. (69)–(71).

C. Solution of the gap equations in the cases of large and small FS's

Explicit solutions of the gap equations depend on the dispersion law of charged quasiparticles in the normal state and on their FS. We analyze below the solutions of these equations for the two cases corresponding to the normal-state hole dynamics described by solutions I and II; see Sec. III.

1. Normal state corresponding to solution I (FS with volume proportional to δ)

We analyze below the case of solution I to get an idea about the possibility of a SC pairing in the case of the small FS. This analysis is going to be rather formal since as we will see the SC solution found for the doping range of the stability of solution I does not satisfy the constraint (48). Nevertheless, it is worthwhile to understand the interrelation between the size and shape of FS and the possibile symmetry of the SC pairing.

We show in Fig. 14 the amplitudes of the SC gap found for the two cases $t'=-0.1$ and $t'=-0.4$. One can see that the gap equations have only the s-wave solution (77) for low and moderate doping and the d-wave solution (76) (with $\Delta=0$) for high doping. For the s-wave solution, the constant term is always larger than the amplitude of the extended s-wave term Δ_0^s. Therefore, the SC gap has no nodes; i.e., the SC order parameter $F_{\mathbf{p}}$ does not change sign within the Brillouin zone (see Fig. 15). It automatically follows that this solution does not fulfill the constraint (48) and thus should be omitted.

For the d-wave solution the constant term is equal to zero (see Fig. 14), and this solution matches the constraint (48). However, the doping range for this d-wave solution is out of the range of the existence of the solution I in the normal state (compare Fig. 14 with Fig. 3) and thus the d-wave solution also cannot be retained.

2. Normal state corresponding to solution II (FS with volume proportional to $1+\delta$)

Let us concentrate now on the normal-state solution II, characterized by the FS close to the observed experimentally. By solving Eq. (79), we have found the superconducting gap of the d-wave symmetry (76) with $\Delta=0$, and this is the only solution which exists for the case of preserved symmetry $k_x \leftrightarrow k_y$. The doping dependence of the amplitude of the SC gap for the three sets of parameters (i) $t'/t=-0.1$, $t''=0$, (ii) $t'/t=-0.4$, $t''=0$, and (iii) $t'/t=-0.38$, $t''/t=0.06$, is shown in Figs. 16, 17, and 18 respectively. [We remind the reader here that set (i) has been chosen to model the FS typical for monolayer cuprates and sets (ii) and (iii) to mimic the situation for bilayer cuprates.] The corresponding wave vector dependences of the SC OP, $F_{\mathbf{k}}$, are shown in Figs. 19 and 20.[103] One can see that the SC OP changes sign in the same manner as the d-wave SC gap; however, in contrast the order parameter is different from zero only in the close vicinity of the FS, indicating that superconducting pairing takes place close to the Fermi level. The condition (48) is fulfilled. We stress here that the interaction responsible for the obtained SC solution is the J interaction as seen from Eq. (79), while the t interaction does not contribute. The reason is that the J and t interactions have different wave vector

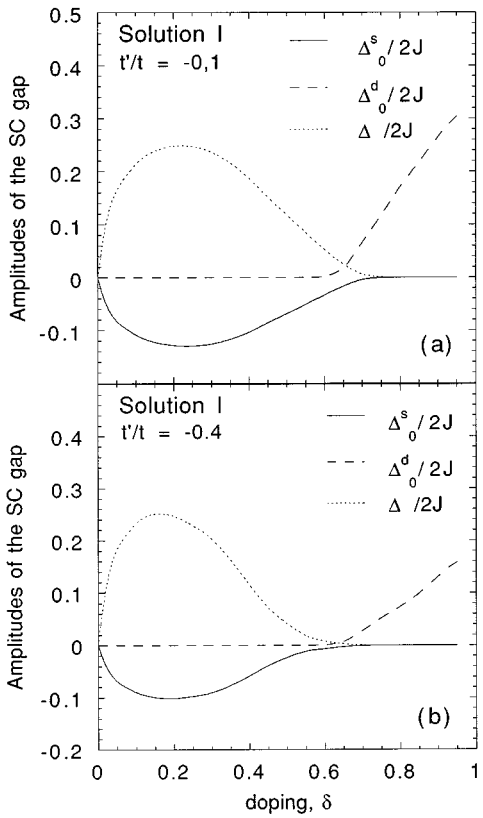

FIG. 14. Amplitudes of the SC gap in the case of solution I. (a) corresponds to $t/J=1.8$, $t'/t=-0.1$ and (b) to $t/J=1.8$, $t'/t=-0.4$.

dependences as far as the $t_{\mathbf{q}}$ interaction is associated with three Green-function lines belonging to the same site and the fourth line belonging to another site, and the $J_{\mathbf{k}-\mathbf{q}}$ interaction is associated with two Green-function lines belonging to the same site and two lines belonging to another site.

Although the amplitudes of the SC gap turned out to be large in all three cases of the above parameters, a strong quantitative difference exists. Namely, we found that the maximum value of Δ_0^d is almost twice larger in the case of $t'/t=-0.4$ than in the case of $t'/t=-0.1$. It should be combined with the observation that for the cases presented in Figs. 17 and 18, the maximum value of Δ_0^d is almost the same although the extensions of the saddle point differ significantly.

To understand the reasons for the very large values of the amplitudes of the d-wave SC gap and for the differences between three cases discussed, let us analyze qualitatively Eq. (79) for the amplitude of the d-wave gap which simplified (at low T) version takes the form

$$1=\frac{1}{N}\sum_{\mathbf{k}}\frac{4J\alpha_{\mathbf{k}}^2}{\sqrt{\tilde{\epsilon}_{\mathbf{k}}^2+(\tilde{\Delta}_0^d\alpha_{\mathbf{k}})^2}}, \tag{81}$$

with an effective dispersion law $\tilde{\epsilon}_{\mathbf{k}}$ and an effective SC gap $\tilde{\Delta}_0^d$ given by

$$\tilde{\epsilon}_{\mathbf{k}}=\frac{\epsilon_{\mathbf{k}\sigma}-\mu}{(1+\delta)/2}, \quad \tilde{\Delta}_0^d=\frac{\Delta_0^d}{(1+\delta)/2}. \tag{82}$$

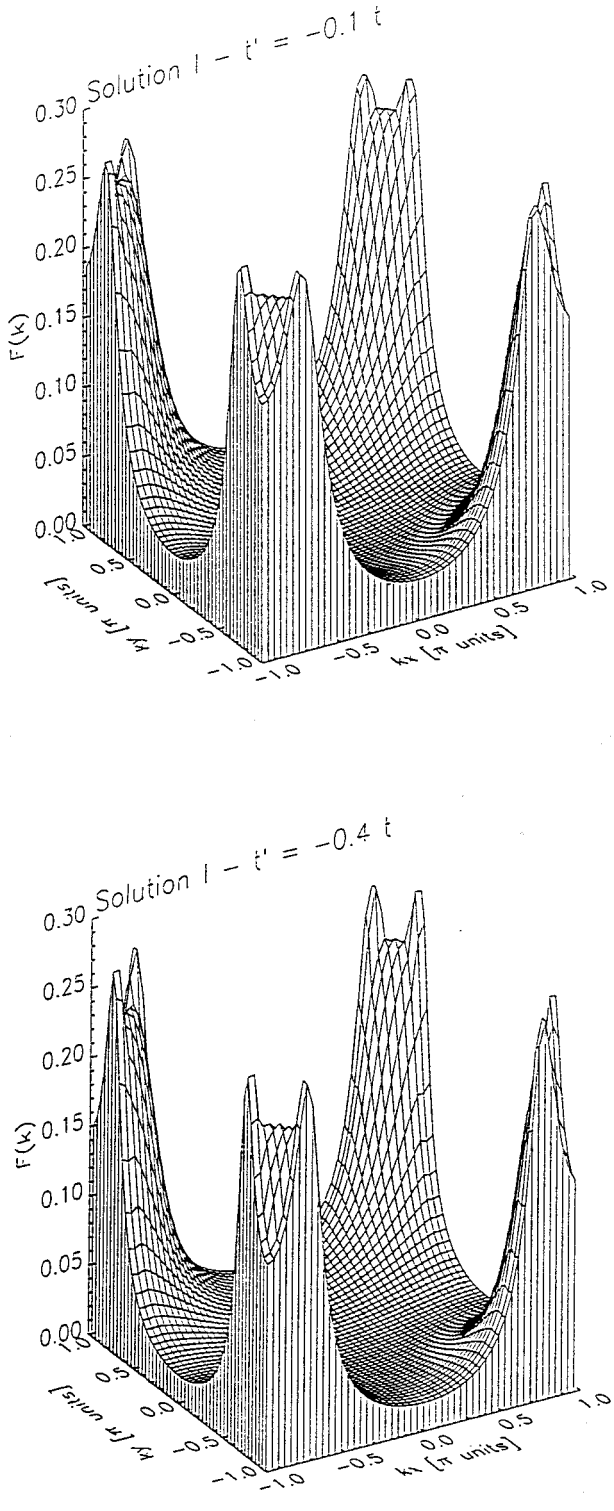

FIG. 15. Superconducting order parameter $F_{\mathbf{k}}$ for solution I.

Let us consider the range of doping around $Z=|\epsilon_F-\epsilon_s|=0$, i.e., the range where the energy distance between the flat part of the normal-state hole spectrum and the Fermi level (FL) is small. A dominant contribution to the sum over $\mathbf{k}$ in Eq. (81) is given by wave vectors around the points $(\pm\pi,0),(0,\pm\pi)$ where, on the one hand, the saddle points in the spectrum $\tilde{\epsilon}_{\mathbf{k}}$ are located and, on the other hand, the effective attractive interaction $J\alpha_{\mathbf{k}}^2$ is maximum. One can characterize the wave vector region where the latter interaction is considerable by a surface sN (the extension of the interaction potential). One can introduce also an effective extension of the saddle point (SP) $\tilde{r}$ as a wave vector area where the effect of the flat part of the spectrum is crucial for the integral (81). This extension is determined by the extension r of the flat part of the spectrum itself and by the wave vector distance between the flat part and the FL, $l \propto(\delta-\delta_c)^2$. Then, a rough estimate of the integral in Eq. (81) gives

$$\tilde{\Delta}_0^d \approx 4J\min(s,r-l). \tag{83}$$

Let us analyze the three cases of parameters: (i), (ii), and (iii).

In the case of $t'/t=-0.1$, $t''=0$, the extension r of the flat part is smaller than s and therefore Eq. (83) transforms to

$$\tilde{\Delta}_0^d \approx 4J(r-l). \tag{84}$$

In such a case, the effect of the SP is sensible and the maximum of the effective gap $\tilde{\Delta}_0^d$ is reached at the doping δ_c at

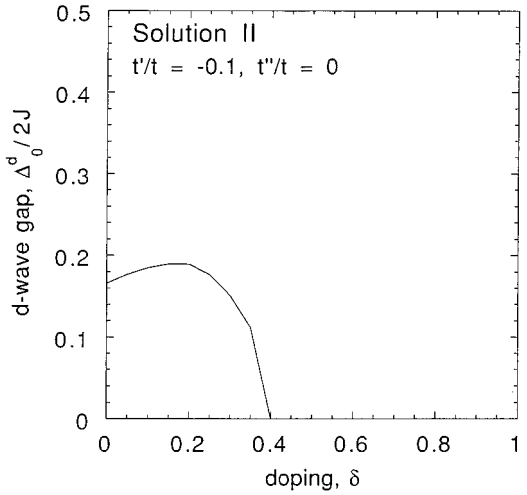

FIG. 16. Amplitude of the d-wave gap (solution II) for $t'/t=-0.1$.

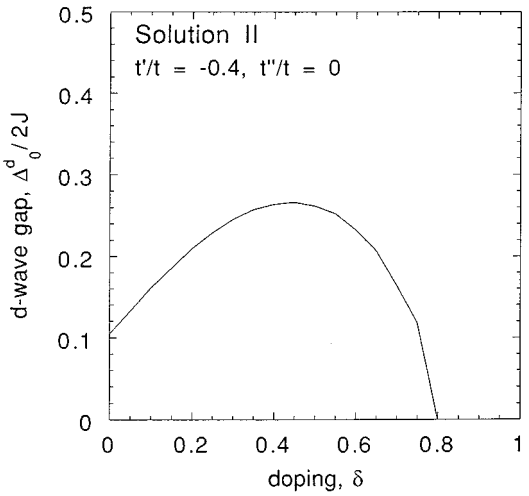

FIG. 17. Amplitude of the d-wave gap (solution II) for $t'/t=-0.4$.

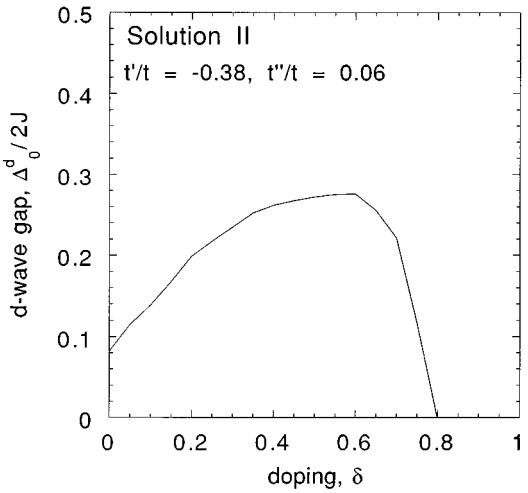

FIG. 18. Amplitude of the d-wave gap (solution II) for $t'/t=-0.38$, $t''/t=0.06$.

which E_F crosses the SP. The value of $\tilde{\Delta}_0^d$ decreases quite quickly when one moves from this doping due to an increase of l. This explains the doping dependence of the effective gap $\tilde{\Delta}_0^d$, obtained by numerical calculations; see Fig. 21 for $t'/t=-0.1$, $t''=0$. The maximum of the true gap, Δ_0^d, is reached at higher doping $\delta=\delta^*>\delta_c$, due to the factor $(1+\delta)/2$; compare the curves for $t'/t=-0.1$ in Figs. 21 and 22.

In both cases $t'/t=-0.4, t''=0$ and $t'/t=-0.38$, $t''=0.06$, the extension r of the flat part is larger than s. Therefore, at the doping $\delta=\delta_c$ one has

$$\tilde{\Delta}_0^d \approx 4Js. \tag{85}$$

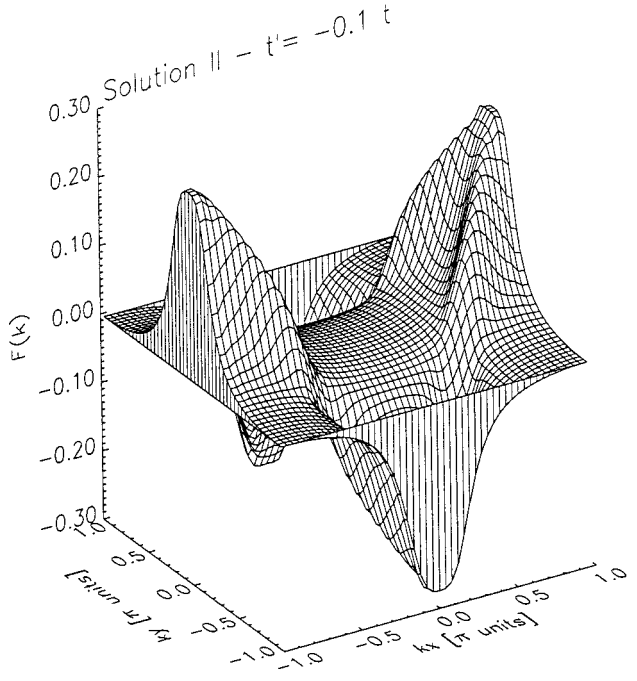

FIG. 19. Superconducting order parameter $F_{\mathbf{k}}$ for solution II and $t'/t=-0.1$.

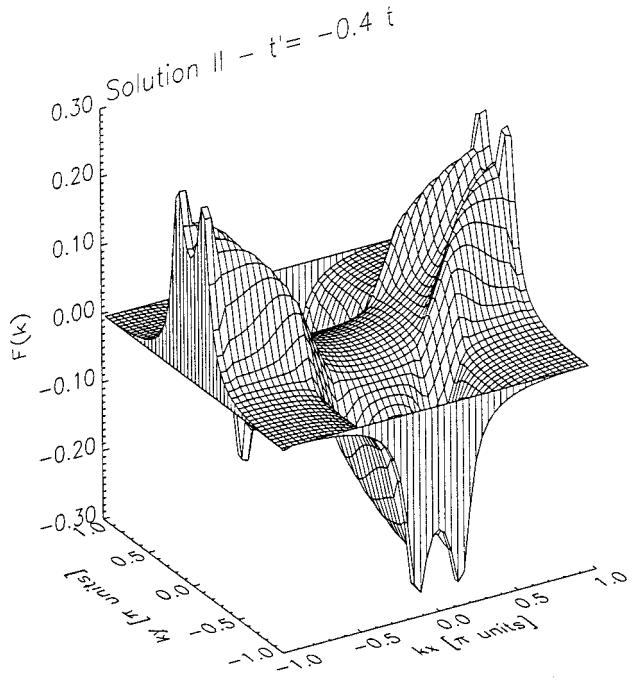

FIG. 20. Superconducting order parameter $F_{\mathbf{k}}$ for solution II and $t'/t=-0.4$.

The same equality is valid for some doping range around δ_c as far as $r-l \geqslant s$. Therefore, the doping dependence of the effective SC gap $\tilde{\Delta}_0^d$ exhibits a kind of plateau or broad maximum. *The high value of the SC gap within this doping range is determined by the value and extension of the effective interaction potential.* Then, with further increasing of $|\delta-\delta_c|$, the quantity $\tilde{r}=r-l$ becomes smaller than s and hence $\tilde{\Delta}_0^d$ is determined by Eq. (83); i.e., it decreases as $\sigma-\alpha(\delta-\delta_c)^2$. This analysis enables us to understand qualitatively the shape of the dependence $\tilde{\Delta}_0^d(\delta)$ obtained by direct calculations and presented in Fig. 21 for the parameters considered. The doping dependence of the true gap Δ_0^d is shown in Fig. 22. The curve is asymmetric: The maximum of Δ_0^d is realized at higher doping than the maximum of $\tilde{\Delta}_0^d$ due to the factor $1+\delta$.

For the parameters corresponding to an intermediate situation, the shape of $\tilde{\Delta}_0^d(\delta)$ evolves continuously between the two cases considered above; see Fig. 21. The maximum value of $\tilde{\Delta}_0^d$ increases until a critical extension of the SP is reached. The maximum value of the true gap Δ_0^d increases even stronger due to the factor $(1+\delta)/2$. Once the equality $\sigma=s$ is reached, a further increase of the extension of the SP singularity, σ, has no influence on $(\tilde{\Delta}_0^d)^{\max}$ which is still determined by Eq. (85). That is why the maximum values of $\tilde{\Delta}_0^d$ are almost the same for the two sets of parameters: $t'/t=-0.4$, $t''=0$, on the one hand, and $t'/t=-0.38$, $t''=0.06$, on the other, although the difference in the extension of the saddle-point singularities is important. The quantity dependent on the extension of the saddle points is the width of the doping range around δ_c where Eq. (85) is fulfilled. The larger is the extension of the SP, the larger is the flat part of $\tilde{\Delta}_0^d(\delta)$. [So far as the extension σ is large in the case $t'/t=-0.38$, $t''=0.06$, the flat part in $\tilde{\Delta}_0^d(\delta)$ is quite

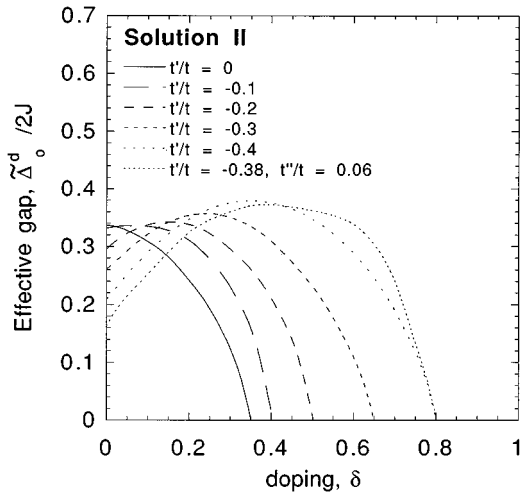

FIG. 21. Doping dependence of the effective d-wave gap $\tilde{\Delta}_0^d$ for different t'/t and t''/t ratios.

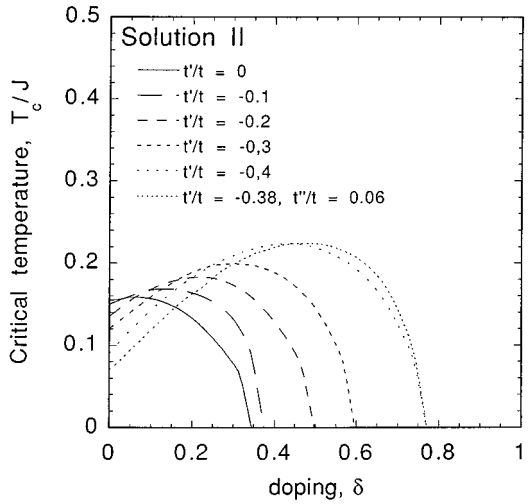

FIG. 23. Critical temperature as a function of doping for different t'/t and t''/t ratios.

large.] These two facts, the saturation of $(\tilde{\Delta}_0^d)^{\max}$ and the increase of the doping range of the plateau in $\tilde{\Delta}_0^d(\delta)$ with an increase of the extension of SP singularity, lead to the doping dependence of the true gap Δ_0^d shown in Fig. 22 for the two cases (ii) and (iii). The optimal doping corresponding to the maximum of Δ_0^d increases with an increase of the extension of the SP singularity. As to the maximum value of Δ_0^d, then in the cases when the saturation of $\tilde{\Delta}_0^d$ is reached, it also increases with increase of the extension of the SP singularity but much weaker than in the ''unsaturated case,'' for it is determined only by the factor $(1+\delta)/2$ which enhances the high-energy part of the plateau.

To complete this discussion we show in Fig. 23 the doping dependence of T_c obtained by numerical solution of Eq. (79). One can see that in the cases when the extension of the SP is smaller than optimal one (LSCO case), the doping dependences of T_c resembles qualitatively the doping dependence of the true SC gap. On the contrary, in approaching the optimal extension this dependence resembles the doping dependence of the effective SC gap, $\tilde{\Delta}_0^d(\delta)$, i.e., $T_c^{\max}$ saturates with increasing the extension. In addition to the interesting effect of the saturation, the latter means first that in the case of the optimal extension (YBCO case), the ratio Δ_0^d/T_c increases with doping, being maximum at optimal doping, and second that this ratio taken at optimal doping is larger in the case of a large extension (YBCO) than in the case of a small extension (LSCO).

Until now we considered the situation where the symmetry $k_x \leftrightarrow k_y$ exists. This corresponds to a tetragonal lattice. We found that the large FS is compatible with the d-wave symmetry of the SC OP and that this is the only type of solution which exists in the case considered. The next point that we would like to analyze is the following. What are the conditions necessary for the existence of mixed $s+d$ or $s+id$ solutions? The answer which we have found is as follows. These solutions appear only in the case when the symmetry $k_x \leftrightarrow k_y$ is broken. This can occur due to a small anisotropy in the dispersion law (and therefore in the FS) or due to the anisotropy in the interaction potential. Both factors can appear as a result of an orthorhombic distortion of the lattice. Even a small anisotropy is enough to drive a solution from the pure d-wave symmetry to the $s+d$ symmetry. However, the amplitude of the s term is small as far as the anisotropy is small. For example, the solution found in the case of a forced anisotropy of the dispersion law

$$\frac{\epsilon_{\mathbf{k}\sigma}}{(1+\delta)/2} = 2t(\cos k_x + \alpha \cos k_y) + 4t' \cos k_x \cos k_y , \quad (86)$$

with $\alpha = 0.95$, is found to be very close to the d-wave solution existing in the case of $\alpha = 1$. The ratio of the amplitudes is $\Delta_0^s/\Delta_0^d \approx 10^{-2}$. Thus, although formally the SC gap has an $s+d$ symmetry in the case of the orthorhombic distortion, the amplitude of the s-wave component is so small that the gap can be considered as having almost pure d-wave symmetry.

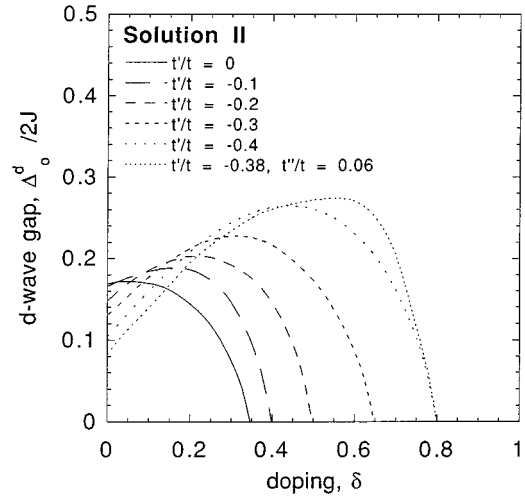

FIG. 22. Amplitude of the true d-wave SC gap as a function of doping for different t'/t and t''/t ratios.

V. DISCUSSION

In the present paper, we have analyzed the evolution of hole dynamics in the CuO_2 plane from low to high concentration of doped holes. We obtained stimulating results for the normal and superconducting states.

A. Normal state

In the normal state we have found two qualitatively different states which we call phase I and phase II. In the case of phase I, the FS is formed by doped holes only whereas copper holes initially present are responsible for localized magnetism. In the case of solution II, the holes on copper become a part of the FS while the system loses the localized magnetic moments associated with the d electrons. The volume of the FS is proportional to δ in the case of solution I and to $1+\delta$ in the case of solution II. A first-order phase transition between them is found at some critical doping $\delta=\delta_0(T)$. The line of first-order phase transitions terminates at some temperature by a critical point.

With lowering the temperature, phase I becomes unstable as far as the spin susceptibility diverges at $\mathbf{k}=\mathbf{Q}_{\mathrm{AF}}$. Therefore, this solution transforms into a LR AF solution I' at $T=0$ and low doping. The AF ground state in its turn is stable only up to critical doping $\delta=\delta_N^{\mathrm{2D}}$. Above this doping, magnons with wave vectors close to Q_{AF} lose their identity and decay into electron-hole pairs.[69] (According to Ref. 69, this concentration is very low, of the order of 0.02–0.04 for relevant values of hopping parameters.) There are two possibilities for the ground state at doping higher than δ_N. The first one is realized if $\delta_N \geqslant \delta_0(0)$. In this case, the first-order phase transition from the LR AF state to the metallic state II occurs at $\delta=\delta_0(0)$, and the FS changes abruptly from the FS with four small pockets centered at $(\pm\pi/2,\pm\pi/2)$ to the FS with large hole pockets centered at $(\pm\pi,\pm\pi)$. The second possibility is realized if $\delta_N<\delta_0(0)$. In this case, for the doping range $\delta_N<\delta<\delta_0(0)$, a spin liquid [or quantum-disordered (QD) state in the classification of Ref. 77] takes place. Properties of the hole subsystem in the latter ground state are a subject of special investigation; anyway the volume of the FS is proportional to δ. At a doping level higher than δ_0, the system exists in the metallic ground state described by solution II. For this solution, the FS is large even at small values of δ; see Fig. 2. The two possibilities discussed above are presented in the schematic phase diagram in Figs. 24(a) and 24(b).

As far as solution I exists only at low doping, the bandwidth of the quasiparticles is very narrow and one can argue that in reality any additional interaction (like impurity scattering, etc.) leads to a localization of holes and makes this state an insulating one. State II with a large bandwidth corresponds to a metallic state. From this point of view, one could interpret the line of the first-order phase transitions discussed above, $\delta=\delta_0(T)$, as a line of metal-insulator phase transitions (this is, however, only a speculation).

We analyzed the metallic state II by solving the equation for the chemical potential self-consistently and found a critical doping δ_c at which the Fermi level crosses the saddle-point singularity. The value of critical doping varies between 0.1 and 0.4 depending on the ratio t'/t. We have also found that in the underdoped regime $\delta<\delta_c$, the Fermi level lies very close to the saddle-point energy. The distance between them, $Z=\epsilon_s-\epsilon_F$, changes very little with doping in the underdoped regime and in a much sharper way in the overdoped regime. This result lets one understand the experimental observation[88] that the distance between the saddle point and the Fermi level is very small (namely is smaller than 30 meV) in a wide region of doping in the underdoped regime of the bilayer compounds (a fact which cannot be understood within the rigid band scheme, as emphasized in Ref. 88.) In correspondence with the weak variation of $|\epsilon_F-\epsilon_s|$ with doping, the FS also changes only a little in the underdoped regime. Such a weak change is also in good agreement with photoemission experiments.

We summarize all transition lines discussed above in the schematic phase diagram presented in Fig. 24.

B. Superconducting state

Summarizing, we have found a short-distance superconducting pairing of $d_{x^2-y^2}$ symmetry. The amplitude of the SC gap at low temperature and the value of the critical temperature are very high. The superconducting pairing has a magnetic origin but the mechanism is different from the exchange by spin waves. The mechanism found is related to the AF interaction between localized spins turning out to be a direct attractive interaction between itinerant charged quasiparticles. The latter point is a consequence of the specific nature of these quasiparticles appearing as a result of strong on-site Coulomb repulsion. On the other hand, the specific kinematic properties of the carriers create a strong constraint on the symmetry of the superconducting order parameter which eliminates all symmetries without nodes and favors strongly the d-wave symmetry. In such a situation the existence of a saddle point close to FL is an additional important factor which provides a maximum value of the effective attractive interaction. Below we discuss certain points crucially important for superconductivity in more detail.

1. Relation between symmetry of the SC pairing and the volume and shape of the FS

The first point is the relation between the symmetry of the SC pairing and the volume and shape of the FS. As we have seen, for the case of the small FS, the solution of the gap equation has s-wave symmetry, while in the case of the large FS, it has d-wave symmetry. The reason is simple. In the case of d-wave symmetry, the effective attractive interaction appearing in the numerator of the gap equation, $J\alpha_{\mathbf{k}}^2$, has a considerable magnitude only around the points $(\pm\pi,0),(0,\pm\pi)$. While SC pairing is possible only for quasiparticles in the vicinity of the FS, there is no significant attraction for them in the case of the small FS and there is a strong attractive interaction when the FS is extended towards these points. On the contrary, in the case of extended s-wave symmetry, the effective interaction has the form $J\gamma_{\mathbf{k}}^2$ and is maximum around $(\pm\pi,\pm\pi),(0,0)$ (while in the case of pure s-wave symmetry, the effective interaction exists everywhere). Therefore extended s-wave symmetry is compatible with the small FS around $(\pm\pi,\pm\pi),(0,0)$. This is a purely geometrical effect which is common for all types of systems regardless of the nature of the quasiparticles creating SC pairs.

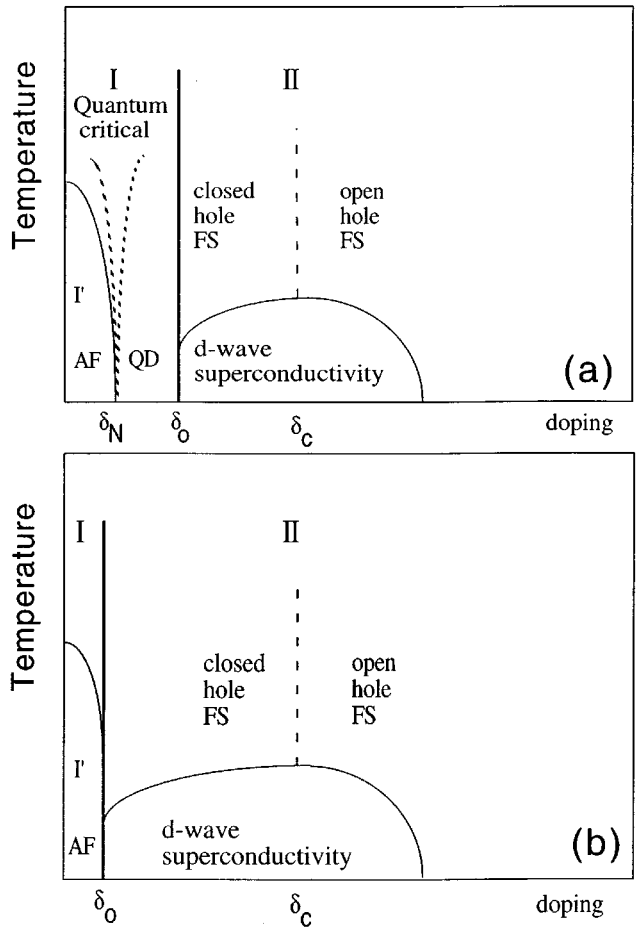

FIG. 24. Schematic phase diagram summarizing our results. The line $\delta=\delta_0$ is the line of the first-order phase transition between the normal states described by solutions I and II. The line $\delta=\delta_c$ is the line of electronic topological transitions. δ_N is the doping of instability of the LR AF ground state. (The existence of the LR AF state at finite T is a consequence of the implied exchange interaction between planes.) We add also the lines which have not been calculated in the paper but which are important for state I, namely, the dashed lines of crossover between different regimes for the 2D localized-spin system, renormalized classical AF regime, quantum-disordered (QD) regime, and quantum critical regime (the classification is given in a correspondence with Ref. 77). The phase diagram (a) corresponds to the case when $\delta_0>\delta_N$ and (b) to the opposite case.

2. Role of the nature of normal-state quasiparticles for the symmetry of the superconducting order parameter

The nature of quasiparticles which are the subjects for pairing is very important. In strong-coupling-limit theories, the quasiparticles in the normal state are associated with Fermi-like LH operators. In weak-coupling-limit theories, they are fermions. Both types of operators are similar for different sites (they anticommute), which results in many common properties like the existence of FS etc. However, they are very different for the same site. Namely, two fermions with different spins can exist on the same site whereas two quasiparticles associated with Lie-Hubbard operators cannot. This is an intrinsic property of the algebra of projection operators; see Eq. (49). This leads to the constraint (48) which eliminates many symmetries of the SC OP. (From the physical point of view this feature appears very natural if one remembers that the appearance of the new type of quasiparticles is related to the strong on-site Coulomb repulsion which obviously prevents the possibility of the existence of two on-site carriers.) This very strong constraint eliminates not only all symmetries without nodes but requires integrally equal parts with positive and negative amplitudes of the OP. It should be emphasized that such a constraint exists for all strong-coupling-limit models as far as they are formulated in terms of LH operators, for the t-J model, for the one-band Hubbard model, for the three-band Hubbard model, etc. Summarizing, almost all symmetries of the SC OP possible in the case of fermions are eliminated in the case when quasiparticles are Fermi-like lieons.

3. Role of the nature of normal-state quasiparticles for the existence of an attractive interaction

On the other hand, the specific nature of the normal-state quasiparticles (lieons) results in the existence of a direct interaction between them, which is hidden in the exchange and the hopping terms of the Hamiltonian. Being momentum dependent, these two types of interaction are attractive for some range of wave vectors of quasiparticles. It is important that the very fact of the existence of such attractions does not depend on the approximation considered. This fact is a consequence of new (in comparison with Bose-Fermi operators) types of vertex blocks characterizing LH operators, which in its turn is a direct consequence of the algebra of LH operators.

The wave vector range of attraction is different for t and J interactions. This results in different symmetries of possible SC pairing associated with pure t and pure J interactions, namely, in isotropic s-wave and d-wave or extended s-wave symmetries, respectively. When these interactions are considered simultaneously, the t interaction does not participate in the creation of the d-wave or extended s-wave pairing, and the J interaction does not in the isotropic s-wave one. As far as only the symmetries with nodes are possible, the antiferromagnetic interaction is a true interaction responsible for the SC pairing in the considered strongly correlated electron system. As far as the amplitude of this interaction is very large, this leads to large value of the superconducting gap.

The attractive interaction $t_{\mathbf{q}}$, although it exists, does not lead to SC pairing. On the contrary, it prevents SC pairing, since in its presence the extended s-wave solution existing for $t=t'=0$ [see Eq. (80)] is replaced by a generalized s-wave pairing with a nonzero constant term. As we discussed above, in the presence of the constant term Δ in the $\mathbf{k}$ dependence of the SC gap, the constraint (48) is not fulfilled that eliminates this SC solution. A possibility to fulfill this constraint (and therefore for the s-wave solution to be allowed) exists only for the very special interrelation between t and t'.

4. Saddle point close to Fermi level: Interrelation between the extension of the saddle point and the maximum value of the SC gap

The next point is a role of the SP and the interrelation between the extension of the saddle point and the optimal

value of the SC gap. We have found that the extension of the saddle point is indeed important (in agreement with a phenomenological idea put forward in Refs. 13 and 14), however, its interrelation with the optimal value of the SC gap is not trivial. The latter increases until some critical extension of the SP is reached and then *remains almost saturated*. This ''saturated'' value of $(\Delta_0^d)^{\max}$ is determined by the amplitude of the exchange interaction and by its extension within the Brillouin zone:

$$(\Delta_0^d)^{\max}=\frac{1+\delta^*}{2}Js, \tag{87}$$

where δ^* is the value of the optimal doping. The critical temperature T_c saturates upon reaching the critical extension of the saddle point as well. (All the features discussed above are valid for the tetragonal lattice symmetry. In the case of the orthorhombic distortion, we have found a weak admixture of the s-wave component such that the symmetry of the SC gap is $s+d$. However, the ratio Δ_0^s/Δ_0^d is so low that there is only a small quantitative difference from the pure d-wave case).

5. Schematic phase diagram

In the main text of the paper, we have analyzed separately the possibility of SC pairing for quasiparticles corresponding to solutions I and II. We have shown that in the case of phase II, the self-consistency equation yields for the SC gap the d-wave symmetry. The SC pairing corresponds to the short-distance pairing. There is no such pairing in the case of phase I since the required constraint (48) is not fulfilled. Focusing on the evolution of the picture with doping from low to moderate doping, one has to keep in mind the change in the character of the normal-state hole dynamics, discussed in Sec. V A. As a result, we can complete our schematic phase diagram by the line $T_c(\delta)$ which terminates at $\delta=\delta_0$, since no superconductivity (given by the mechanism considered) exists for phase I. In correspondence with this phase diagram, the disappearance of the short-distance superconductivity should be quite sharp at low doping due to the abrupt disappearance of the ''metallic'' solution II. It has to be noted that the question of the existence of superconductivity in the left part of the phase diagram (corresponding to phase I) is open. As we discussed in Sec. IV A, the possibility of attraction mediated by a virtual magnon exists for this phase that in principle could lead to a long-distance SC pairing. (However there is a problem of the existence itself of such an interaction in the phase without LR ordering, as we have discussed in Sec. IV A). We also leave open the question of the value of δ_0 as far as it should be determined at low T by comparing free energies for the metallic state II and for the quantum disordered state. To be reliable such calculations should be done in a rather high approximation due to the well-known sensibility of the free energy. Crude estimations show however that δ_0 is generally larger than δ_N and that its value depends much on ratio t'/t, namely it decreases when $|t'/t|$ increases (t'/t being negative).

We would like to note also that as far as the phase transition between the states I and II is of first order, this makes the possibility of finding domains of another phase existing on both sides from $\delta=\delta_c$. This could explain the results of Mössbauer spectroscopy[104,105] and of muon-spin-rotation studies,[106] where the phase separation between local magnetic and local nonmagnetic (superconducting) regions has been found in the SC states of $YBa_2Cu_3O_{6+x}$ $(0\leqslant x\leqslant 1)$,[104,106] of $YBa_2(Cu_{0.94}Zn_{0.06}O_{6+x}$ $(0\leqslant x\leqslant 1)$,[105] and of $La_{2-x}Sr_xCuO_4$.[106]

ACKNOWLEDGMENT

We are kindly grateful to Pierre Pfeuty for fruitful discussions.

APPENDIX: HOLE AND SPIN GREEN FUNCTIONS IN THE DOPED AF STATE

In the case of a rigid two-sublattice AF structure of the ground state, all characteristics describing the system are 2×2 matrices. The Larkin equation has the matrix form

$$\hat{G}=(\hat{I}-\hat{\Sigma}\hat{V})^{-1}\hat{\Sigma}, \tag{A1}$$

where $\hat{V}$ is a matrix of the interaction potential and $\hat{\Sigma}$ is the matrix of the irreducible part. The spin irreducible part in a zero-order approximation is given by

$$\hat{\Sigma}^{s(0)}=\begin{bmatrix} \dfrac{b_A^{\sigma\sigma'}}{h_A-i\omega_n^B} & 0 \\ 0 & \dfrac{b_B^{\sigma\sigma'}}{h_B-i\omega_n^B} \end{bmatrix}, \tag{A2}$$

where $b^{\sigma\sigma'}$ is determined as in Eq. (21) and is different for different sublattices, and $h_{A,B}$ are internal magnetic fields conjugated to the AF order parameter (the values of $h_{A,B}$ is proportional to $\langle S^z\rangle_{A,B}^{(0)}$). The matrix of the interaction potential for the case of the spin Green function is written as

$$\hat{V}^s=\begin{bmatrix} V_{AA}^s & V_{AB}^s \\ V_{BA}^s & V_{BB}^s \end{bmatrix}=\begin{bmatrix} 0 & -J_{\mathbf{k}} \\ -J_{\mathbf{k}} & 0 \end{bmatrix}, \tag{A3}$$

if we neglect the intrasublattice interaction and take into account only the intersublattice AF interaction. When $\Sigma^{s(0)}$ is dominant in comparison with other contributions to the spin irreducible part (i.e., in the pure AF state of the undoped cuprates), the spin Green function given by Eq. (A1) acquires the form

$$\hat{G}^s=\hat{K}^s\hat{b}, \tag{A4}$$

$$\hat{K}^s=\begin{bmatrix} K_{AA} & K_{AB} \\ K_{AB} & K_{BB} \end{bmatrix}, \quad \hat{b}=\begin{bmatrix} b_A^{\sigma\sigma'} & 0 \\ 0 & b_B^{\sigma\sigma'} \end{bmatrix}, \tag{A5}$$

$$K_{AA}(k,i\omega_n)=\frac{u_{\mathbf{k}}^2}{\omega_{\mathbf{k}}-i\omega_n}+\frac{v_{\mathbf{k}}^2}{\omega_{\mathbf{k}}+i\omega_n}, \tag{A6}$$

$$K_{BB}(k,i\omega_n)=\frac{v_{\mathbf{k}}^2}{\omega_{\mathbf{k}}-i\omega_n}+\frac{u_{\mathbf{k}}^2}{\omega_{\mathbf{k}}+i\omega_n}, \tag{A7}$$

$$K_{AB}(k,i\omega_n)=u_{\mathbf{k}}v_{\mathbf{k}}\left\{\frac{1}{\omega_{\mathbf{k}}-i\omega_n}+\frac{1}{\omega_{\mathbf{k}}+i\omega_n}\right\}. \tag{A8}$$

In Eqs. (A6)–(A8), the magnon dispersion law $\omega_{\mathbf{k}}$ and the functions $u_{\mathbf{k}}$ and $v_{\mathbf{k}}$ are given by

$$\omega_{\mathbf{k}}=bJ_0\sqrt{1-\gamma_{\mathbf{k}}^2}, \tag{A9}$$

$$u_{\mathbf{k}}^2, v_{\mathbf{k}}^2=\frac{1}{2}\left(1\pm\frac{1}{\sqrt{1-\gamma_{\mathbf{k}}^2}}\right), \tag{A10}$$

where

$$b=b_A^{\sigma\sigma'}=-b_B^{\sigma\sigma'}=2\langle S^z\rangle_{A,B}^{(0)}=1-\delta \tag{A11}$$

and $\gamma_{\mathbf{k}}$ is determined by Eq. (14). Expressions (A6)–(A10) are the usual spin wave equations for the spin Green function in the pure AF state; see, for example, Ref. 56. Note that in the formalism of the DT for Lie-Hubbard operators they correspond to a zero-order approximation for the spin irreducible part.

The hole Green function in the AF state is a 2×2 matrix as well. It is given by the Larkin equation (A1) with a hole irreducible part which in a zero-order approximation is written as

$$\hat{\Sigma}_{0\sigma}^{h(0)}=\begin{bmatrix}\dfrac{b_A^{\sigma 0}}{-\mu_A-i\omega_n^F} & 0\\ 0 & \dfrac{b_B^{\sigma 0}}{-\mu_B-i\omega_n^F}\end{bmatrix}, \tag{A12}$$

where $b^{\sigma 0}$ is determined by Eq. (18), and is given by

$$b_{A,B}^{\sigma 0}=\langle X^{00}+X^{\sigma\sigma}\rangle_{A,B}. \tag{A13}$$

The matrix of the interaction potential for the hole Green function is written as

$$\hat{V}^h=-\begin{bmatrix}t'_{\mathbf{k}} & t_{\mathbf{k}}\\ t_{\mathbf{k}} & t'_{\mathbf{k}}\end{bmatrix}. \tag{A14}$$

The term in the denominator of the Larkin equation responsible for the $\mathbf{k}$ dependence of the hole Green function and of its poles depends strongly on values of the first-order cumulants $b_{A,B}^{\sigma 0}$ entering in Eq. (A12). To calculate their values, let us assume that the spins are up $(\sigma=1)$ on sublattice A and down $(\sigma=-1)$ on sublattice B. It means that $\langle X^{-1-1}\rangle_A=\langle X^{11}\rangle_B=0$ and therefore $\langle X^{11}\rangle_A=\langle X^{-1-1}\rangle_B=1-\delta$. Then, one has from Eq. (A13)

$$b_A^{10}=b_B^{-10}=1, \tag{A15}$$

$$b_B^{10}=b_A^{-10}=\delta, \tag{A16}$$

so that the first-order cumulant $b^{\sigma 0}$ is equal to unity for a lattice site belonging to one sublattice, but is vanishingly small at low δ for a site belonging to another sublattice. Therefore, for low δ, the zero-order spin irreducible part is written as

$$\hat{\Sigma}_{01}^{h(0)}\approx\begin{bmatrix}\dfrac{1}{-\mu_A-i\omega_n^F} & 0\\ 0 & 0\end{bmatrix}. \tag{A17}$$

If one neglects nearest-neighbor hopping in the matrix $\hat{V}^h$ given by Eq. (A14), i.e., if one puts $t'_{\mathbf{k}}=0$, then one gets from the Larkin equation

$$\hat{G}_{0\sigma}^h=\Sigma_{0\sigma}^{h(0)}. \tag{A18}$$

The latter means that the holes are not propagating quasiparticles in the pure t-J model. If $t'\neq 0$, one obtains for the diagonal components of the hole Green function the following expression:

$$G_{ff}^h=\frac{1-O(\delta)}{\epsilon_{\mathbf{k}\sigma}^f-\mu-i\omega_n^F}\quad (f=A,B), \tag{A19}$$

$$\epsilon_{\mathbf{k}\sigma}^f=\alpha\gamma_{\mathbf{k}}^2+\beta\gamma_{2\mathbf{k}}, \tag{A20}$$

$$\alpha=8t'\pm\frac{\delta t^2}{2(2J-t')},\quad \beta=-2(t'-2t''). \tag{A21}$$

(t'' is a hopping term corresponding to third neighbors.)

In this case, the holes are propagating quasiparticles with the dispersion law (A20). It is the known result: Such a dispersion law for one hole on the AF background has been obtained earlier in the t-J model (see, for example, Refs. 73, 74, 75, and 69). Here we have shown how this result arises in the DT for Lie-Hubbard operators, since we wish to describe all possible phases within the same formalism.[107]

Thus, a propagation of the doped holes on the AF background is only possible within the same sublattice. Such a propagation occurs due to the hopping to the next nearest neighbors as we have shown above or through virtual spin-flip processes.[74,75] In the former case, the band parameters α and β are determined by Eq. (A21). In the latter case, α and β are proportional to J.[75] For realistic values of the parameters, the dispersion law (A20) is characterized by minima located at the points $(\pm\pi/2,\pm\pi/2)$.

[1] A. Kampf and J.R. Schrieffer, Phys. Rev. B **41**, 6399 (1990).
[2] P. Monthoux and D. Pines, Phys. Rev. B **47**, 6065 (1993).
[3] T. Dahm, J. Erdmenger, K. Scharnberg, and C.T. Rieck, Phys. Rev. B **48**, 3896 (1993).
[4] R. Fehrenbacher and M.R. Norman, Phys. Rev. Lett. **74**, 3884 (1995).
[5] D.M. Newns, C.C Tsuei, and P.C. Pattnaik, Phys. Rev. B **52**, 13 611 (1995).
[6] Y. Ohachi and H. Shiba, J. Phys. Soc. Jpn. **62**, 2783 (1993).
[7] E. Dagotto, and A. Nazarenko, A. Moreo, Phys. Rev. Lett. **74**, 310 (1995).
[8] V.I. Belinicher, A.L. Chernyschev, A.V. Dotschenko, and O.P. Shushkov, Phys. Rev. B **51**, 6076 (1995).
[9] B.O. Wells *et al.*, Phys. Rev. Lett. **74**, 964 (1995).
[10] C.G. Olson *et al.*, Science **245**, 731 (1989).
[11] R. Liu *et al.*, Phys. Rev. B **45**, 5615 (1992); **46**, 11 056 (1992).
[12] R. Gofron *et al.*, J. Phys. Chem. Solids **54**, 1193 (1993).
[13] A.A. Abrikosov, J.C. Campuzano, and K. Gofron, Physica C **214**, 73 (1993).
[14] K. Gofron *et al.*, Phys. Rev. Lett. **73**, 3302 (1994).
[15] D.M. King *et al.*, Phys. Rev. Lett. **70**, 3159 (1993).
[16] D.M. King *et al.*, Phys. Rev. Lett. **73**, 3298 (1994).
[17] D.S. Dessau *et al.*, Phys. Rev. Lett. **71**, 2781 (1995).
[18] Z.X. Shen *et al.*, Science **267**, 343 (1995).

[19]P. Aebi *et al.*, Phys. Rev. Lett. **72**, 2757 (1994).
[20]H. Ding *et al.*, Phys. Rev. Lett. **76**, 1533 (1996).
[21]Bi2212 has a face-centered orthorhombic cell with two inequivalent Cu sites per plane which can generate a π,π foldback.
[22]P.M. Gehring *et al.*, Phys. Rev. B **44**, 2811 (1991).
[23]J. Rossat-Mignod *et al.*, Physica C **86**, 185 (1991).
[24]P. Bourges *et al.*, Physica B **215**, 30 (1995).
[25]The characteristics measured by inelastic neutron scattering is a $\mathbf{q}$ width of $\mathrm{Im}\chi(\mathbf{q},\omega)$ around $\mathbf{q}=\mathbf{Q}_{\mathrm{AF}}$ where the latter is peaked. As far as this $\mathbf{q}$ width does not depend on ω in the metallic state above T_c, it gives (after deconvolution based on the Kramers-Kronig relations) a value of the correlation length.
[26]H.F. Fong *et al.*, Phys. Rev. Lett. **75**, 316 (1995).
[27]P. Bourges *et al.*, Phys. Rev. B **53**, 876 (1996).
[28]H.A. Mook *et al.*, Phys. Rev. Lett. **70**, 3490 (1993).
[29]C. Vettier *et al.*, Phys. Scr. **T29**, 110 (1989).
[30]J. Rossat-Mignod *et al.*, in *Dynamics of Magnetic Fluctuations in High-Temperature Superconductors*, edited by G. Reiter, P. Horsch, and G.C. Psaltakis (Plenum Press, New York, 1990), p. 35.
[31]J. Rossat-Mignod *et al.*, Physica B **163**, 4 (1990).
[32]J. Rossat-Mignod *et al.*, Physica B **169**, 58 (1991).
[33]J. Rossat-Mignod *et al.*, Physica B **180-181**, 383 (1991).
[34]J. Rossat-Mignod *et al.*, Physica B **194-196**, 2131 (1994).
[35]J. Rossat-Mignod *et al.*, Physica B **199-200**, 281 (1994).
[36]J. Rossat-Mignod *et al.*, Physica C **185-189**, 86 (1991).
[37]J. Rossat-Mignod *et al.*, Phys. Scr. **45**, 74 (1992).
[38]J. Rossat-Mignod *et al.*, in *Selected Topics in Superconductivity*, edited by L.C. Gupta and M.S. Multani, Frontiers in Solid State Science (World Scientific, Singapore, 1993), p. 265.
[39]K.A. Moler, D.J. Baar, J.S. Urbach, R. Liang, W.N. Hardy, and A. Kapitulnik, Phys. Rev. Lett. **73**, 2744 (1994).
[40]J.H. Xu, J.L. Shen, J.H Miller, and C.S. Ting, Phys. Rev. Lett. **73**, 2492 (1994).
[41]D.J. Scalapino, Phys. Rep. **250**, 329 (1995).
[42]A. Subdo and S.P. Strong, Phys. Rev. B **51**, 1338 (1995).
[43]F.P. Onufrieva, Physica C **251**, 348 (1995).
[44]F.C. Zhang and T.M. Rice, Phys. Rev. B **37**, 3759 (1988).
[45]M. Hybertsen, E.B. Stechel, M. Schluter, and D.R Jennison, Phys. Rev. B **41**, 11 068 (1990).
[46]H. Eskes, G.A. Sawatsky, and L.F. Feiner, Physica C **160**, 424 (1989).
[47]Actually, as shown in recent papers (Ref. 48), the localized-spin state of the plaquette in CuO_2 plane is a superposition of states corresponding to a localized spin on copper and to a localized spin on oxygen, but it is not important for the present aim. We use sometimes the term ''localized spins on Cu'' just to simplify the terminology.
[48]V.I. Belinicher and A.L. Chernyschev, Phys. Rev. B **47**, 390 (1993); **49**, 9746 (1994); **53**, 335 (1996).
[49]A possible role of a Van-Hove singularity close to the Fermi level for high-T_c superconductivity in cuprates has been discussed rather early in Refs. 50–53.
[50]J.E. Hirsh and D.J. Scalapino, Phys. Rev. Lett. **56**, 2735 (1986).
[51]J. Labbe and J. Bok, Europhys. Lett. **3**, 1225 (1987).
[52]J. Friedel, J. Phys. Condens. Matter **1**, 7757 (1989).
[53]R.S. Markiewicz and B.G. Giessen, Physica C **160**, 497 (1989).
[54]V.G. Vaks, A.I. Larkin, and S.A. Pikin, Zh. Eskp. Teor. Fiz. **53**, 281 (1967) [Sov. Phys. JETP **26**, 188 (1968)]; **53**, 1089 (1967) [**26**, 647 (1968)].
[55]R.O. Zaitsev, Sov. Phys. JETP **43**, 574 (1976).
[56]Yu.A. Izyumov, Ph. Kassan-Ogli, and Yu.N. Skryabin, *Field Methods in Theory of Ferromagnetism* (Science, Moscow, 1974); Yu. A. Izyumov and Yu. Skryabin, *Statistical Mechanics of Magnetically Ordered Systems* (Consultants Bureau, New York, 1989).
[57]F.P. Onufrieva and J. Rossat-Mignod, Phys. Rev. B **52**, 7572 (1995).
[58]In the initial papers 44–46, the two-hole state has been considered as corresponding to the singlet of the hole on copper and the hole on oxygen (Zhang-Rice singlet) and the single-hole states as corresponding to the copper-hole states. Later it was shown that in fact the localized-spin states are superpositions of the states corresponding to the localized spin on copper and to the localized spin on oxygen and the singlet state is a superposition of different singlet states; see Ref. 48.
[59]In Eq. (7), the upper sign corresponds to the case when both operators on the left hand are Fermi-like, while the lower sign stands for the cases when at least one of them is Bose-like. For the case of the *t-J* model, there are two Bose-like nondiagonal operators X^{1-1} and X^{-11}, four Fermi-like nondiagonal operators X^{01}, X^{10}, X^{-10}, and X^{0-1}, and three diagonal Bose-like operators X^{00}, X^{11}, and X^{-1-1}.
[60]The exact algebra (6)–(8) would be preserved when using the auxiliary representation in terms of Bose-Fermi operators only in the case of an exact treatment of the local constraint forced artificially which is practically impossible.
[61]V.M. Agranovich, Sov. Phys. JETP **37**, 307 (1960); A.S. Davydov, *Theory of Molecular Excitons* (Plenum Press, New York, 1971).
[62]F. Onufrieva, Sov. J. Low Temp. Phys. **3**, 512 (1977).
[63]The spin operators are a certain case of Bose-like projection operators. In the case $S=1/2$ they can be presented as $S^+=X^{1/2-1/2}$, $S^-=X^{-1/2,1/2}$, and $S^z=\frac{1}{2}(X^{11}-X^{-1-1})$. In the case of arbitrary S, the set of operators describing the system is composed of the operators presenting the Lie algebra SU(n), $n=2S+1$. They can be chosen as a complete set of the projection operators [X^{pq} with $p,q=\pm S,\pm(S-1),\pm(S-2),\ \ldots$] or as a set of the spin operators ($O_1^m=S^m$ with $m=0,\pm1,$), the quadrupolar operators (O_2^m with $m=0,\pm1,\pm2,\ldots$), and the tensorial operators of rank $2S$ (O_{2S}^m with $m=0,\pm1,\ldots\pm2S$). The operators of the two sets are related linearly.
[64]In two limiting cases the algebra of X operators can be approximately reduced to the algebra of Bose or Fermi operators, first, when the occupation numbers of excited states are negligibly small. In this case, the commutation relations for conjugated operators can be represented as $[X_i^{\lambda\mu},(X_i^{\lambda\mu})^+]=X_i^{\lambda\lambda}-X_i^{\mu\mu}=1-0(N_{i\mu})\approx1$ (implying that $|\lambda\rangle$ is a ground-state level). Second, it can be reduced when the number of states of the cluster is very large. In this case, the quantum models can be reduced to the corresponding classical ones and then they can be described by Bose operators. Indeed, the intramolecular excitations (librations and vibrations) in classical molecular crystals, the spin fluctuations in the limit $S\to\infty$, etc., are bosons.
[65]In the case of a localized-spin system with $S>1/2$, the importance of the correct treatment of the algebra SU($2S+1$) has been demonstrated in Refs. 66–68. It was shown that once the Hamiltonian of the localized-spin system includes any term out of the subalgebra SU(2) (for example, a single-ion anisotropy, a quadrupolar exchange interaction, etc.), all operators of the complete algebra SU($2S+1$) join to form the ground state, the fluctuations above it, the correlation functions, etc. The physics of

such a localized-spin system becomes untrivial, the ground state is determined by the superposition of the spin and tensorial order parameters, the variety of phases with different type of ordering increases enormously, the quasiparticles are no more the spin fluctuations, the specific phase transitions occur, a specific type of quantum critical behavior is observed, etc.

[66]F. Onufrieva, Sov. Phys. JETP **62**, 1311 (1985).

[67]F. Onufrieva, Sov. Phys. JETP **68**, 516 (1989).

[68]F. Onufrieva, J. Phys. Condens. Matter **2**, 6045 (1990).

[69]F.P. Onufrieva, V.P. Kushnir, and B.P. Toperverg, Physica C **218**, 463 (1993); Phys. Rev. B **50**, 12 935 (1994).

[70]In the diagrammatic technique for LH operators, Green functions of LH operators, Fermi-like or Bose-like type, let us say $G^{pq}=\langle\langle X^{pq}_{\mathbf{k}}|X^{qp}_{-\mathbf{k}}\rangle\rangle_{i\omega_n}$, are related to some effective Green functions of Fermi-type or Bose-type, K^{pq}, describing effective fermions or bosons with the same dispersion laws see Ref. 56. In zero order approximation for irreducible part relation between them is given by $G^{pq}=b^{pq}K^{pq}$, so that the first-order cumulant $b^{pq}=\langle X^{pp}_i \pm X^{qq}_i\rangle$ accompanies the physical Green function G^{pq} ($+$ stands for Fermi-type X^{pq} operator and $-$ for Bose-type).

[71]For the case considered, the low-temperature limit $T/\mu \ll 1$ is fulfilled for all range of parameters of interest.

[72]We neglect here, in comparison with Ref. 57, the contribution related to the spinon subsystem, for its intensity is proportional to the bandwidth of the spinons and is very small compared to the other contributions.

[73]J. Inoue and S. Maekawa, Mod. Phys. Lett. **3**, 1191 (1989); J. Phys. Soc. Jpn. **59**, 2110 (1990); **59**, 3467 (1990).

[74]R. Eder and K. Becker, Z. Phys. B **78**, 219 (1990).

[75]G. Martinez and P. Horsch, Phys. Rev. B **44**, 317 (1991).

[76]The higher-order terms in the spin irreducible part Σ^s considered for state II in Ref. 57 are important to describe the spin dynamics but do not change the discussed tendency determined by the static term (22).

[77]S. Chakravarty, I. Halperin, D. Nelson, Phys. Rev. B **39**, 2344 (1989).

[78]L.F. Mattheiss, Phys. Rev. Lett. **58**, 1028 (1987).

[79]J. Yu *et al.*, Phys. Lett. A **122**, 203 (1987).

[80]J. Yu *et al.*, Physica C **152**, 273 (1988).

[81]T.E. Mason *et al.*, Phys. Rev. Lett. **68**, 1414 (1992).

[82]Q. Si *et al.*, Phys. Rev. B **47**, 9055 (1993).

[83]R.J. Radtke *et al.*, Phys. Rev. B **48**, 15 957 (1993).

[84]C.G. Olson *et al.*, Phys. Rev. B **42**, 381 (1990).

[85]The flatness of the observed experimental bands is certainly a correlation effect. As we show in Ref. 87, it arises due to some scattering processes near an electronic topological transition. In the present paper we only approximately simulate the effect of flatness in the bare spectrum.

[86]R.J. Radtke and M.R. Norman, Phys. Rev. B **50**, 9554 (1994).

[87]F. Onufrieva and P. Pfeuty (unpublished).

[88]R. Liu *et al.*, Phys. Rev. B **52**, 553 (1995).

[89]We use here the ratio $t/J=1.8$ as in the previous paper (Ref. 57) and the experimental estimation for the in-plane exchange interaction $J\approx 120$ meV (Refs. 90–92).

[90]K.B. Lyons *et al.*, Phys. Rev. Lett. **60**, 732 (1988).

[91]S. Shamoto *et al.*, Phys. Rev. B **48**, 13 817 (1993).

[92]S.M. Hayden, G. Aeppli, T.G. Perring, H.A. Mook, and F. Dogan (unpublished).

[93]P.S. Pattnaik *et al.*, Phys. Rev. B **45**, 5714 (1992); D.M. News *et al.*, Phys. Rev. Lett. **73**, 1695 (1994).

[94]In Ref. 93, anomalies in transport properties have been discussed based on numerical calculations of $\tau^{-1}(\omega)$ near the van Hove-singularity which have given $\tau^{-1}(\omega)\propto\omega$. As we show in Ref. 87, more accurate analytical calculations give a dependence corrected by logarithm, $\tau^{-1}(\omega)\propto\omega\ \ln\omega$, and therefore the behavior of the transport properties should be reanalyzed. It should be also noted that an interrelation between the ω dependence of τ^{-1} and the temperature dependence of the resistivity is not trivial (see, for example, Ref. 95), so that more deliberate calculations of the resistivity should be done.

[95]R. Hlubina and M. Rice, Phys. Rev. B **51**, 9253 (1995).

[96]I.M. Lifshitz, Zh. Eskp. Teor. Fiz. **38**, 1569 (1960) [Sov. Phys. JETP **11**, 1130 (1960)].

[97]A.A. Varlamov, V.S. Egorov, and A. Pantsulaya, Adv. Phys. **38**, 465 (1989).

[98]V.Yu. Yushankai, N.M. Plakida, and P. Kalinay, Physica C **174**, 401 (1991); N.M. Plakida, V.Yu. Yushankai, and I.V. Stasyuk, *ibid.* **160**, 80 (1991).

[99]Yu.A. Izyumov, B.M. Letfulov, E.V. Shipitsyn, M. Bartkowiah, and K.A. Chao, Phys. Rev. B **46**, 15 697 (1992).

[100]As usual in the DT for X operators, in the first stage the solid lines in the vertex blocks (here the double solid lines) correspond to zero-order Green functions determined by the on-site Hamiltonian H_0; these Green functions have no wave vector dependence. In the later stage, however, they are replaced by ''dressed'' Green functions which are **k** dependent; see Refs. 56 and 57.

[101]R.O. Zaitsev and V.A. Ivanov, Physica C **153-155**, 1295 (1988).

[102]The graphs in Figs. 11 and 12 correspond to the first-order approximation with respect to $1/z$, as far as they contain one summation over wave vectors; see Ref. 56.

[103]For the case of the parameters $t'/t=-0.38$, $t''/t=0.06$, a wave vector dependence of $F_{\mathbf{k}}$ is pactically the same as in Fig. 19.

[104]J.A. Hodges, P. Bonville, P. Imbert, G. Jehanno, and P. Debray, Physica C **184**, 270 (1991).

[105]J.A. Hodges, P. Bonville, P. Imbert, D. Colson, N. Genand-Riondet, and A. Pinatel-Philippot, Physica C **218**, 272 (1993).

[106]Ch. Niedermayer, C. Bernhard, and J.I. Budnick, J. Magn. Magn. Mater., **140-144**, 1287 (1995).

[107]Note that within the formalism of auxiliary representation for HO's, in order to describe the LR state and the state without LR ordering it is necessary to change the type of representation. This does not allow one to describe the system as a whole within the same theory.